Insole Energy Harvesting

by

Cemalettin Kaplan

A thesis
presented to the University of Waterloo
in fulfillment of the
thesis requirement for the degree of
Master of Applied Science
in
Mechanical and Mechatronics Engineering

Waterloo, Ontario, Canada, 2017

I hereby declare that I am the sole author of this thesis. This is a true copy of the thesis, including any required final revisions, as accepted by my examiners.

I understand that my thesis may be made electronically available to the public.

ABSTRACT

Various energy harvesting techniques have been studied extensively to power portable devices. Each technique has proven to have advantages and disadvantages. Generating energy from human walking is an important energy harvesting application area. Piezoelectric harvesters have come to dominate this area in the last decade, in particular, those that employ polyvinylidene fluoride PVDF and PZT (Lead Zirconate Titanate). However, the low power conversion efficiency of PVDF and durability limitations of PZT have hampered the progress of insole energy harvesters This project is an attempt to generate new options for insole energy harvesters to overcome those limitations. It compares the performance of three classes of insole energy harvesters:

- A baseline harvester employing Terpolymer of P(VDF-TrFE-CFE), a high durability and high fficiency piezoelectric polymer.
- A harvester employing a newly developed ferroelectric material, cellular polypropylene (PP).
- A harvester employing a composite made of Terfenol-D, the magnetostrictive material, and polyurethane, a soft polymer.

Insole energy harvesters were designed to convert to electrical energy the potential energy (pressure) realized in the heel during the heel strike stage of walking. The harvesters were fabricated and tested experimentally to measure their output power under identical test conditions. Results show PP harvesters outperform all others. A non-laminated PP harvester produced 617 μW output power under sinusoidal force at 2 g acceleration.

The project also analyzed the rectification and power management of output power.The efficiency of an off-the-shelf power management chip designed for energy harvesters, LTC3588-1, was found to be less than 10% while that of a custom circuit made of silicon diodes and a switching power supply was found to be better than 90%. Because the available power is low, sub milliwatt, it is important to match the impedance of the harvester to that of the power management circuit, to minimize ON-resistance, and current backflows.

Acknowledgements

Here I would like to thank a couple of people for their invaluable guidance and experience that make this project easier and my study meaningful, thank you...

- Dr. Mustafa Yavuz, my supervisor, for accepting me to study with his group.
- Dr. Eihab Abdel Rahman, my cosupervisor, for giving me the chance to work with the project that is cooperated with NSERC Engage and Vestigo Corporation and the endless support and patience.
- Dr. John Montesano and Dr. William Melek for serving on my dissertation committee.
- Dr. Sarbast Rasheed for his guidance and serving on my dissertation committee.
- Sangtak Park for his technical help and guidance.
- Hamid Nafisi for his help.
- Amirool Ababakor for his help and other group members for their peaceful lab environment and friendship.
- My Family for their unconditional support and love.
- God, the most Merciful and Gracious who has provided all things I have and not despite my unworthiness.

Table of Contents

List of Figures

List of Tables

Nomenclatures

PP	Polypropylene
PVDF	Polyvinylidene fluoride
PU	Polyurethane
PZT	Lead zirconate titanate
ppm	Part per million
W	Power
d_{33}	Piezoelectric coefficient
$S_3(t)$	Strain
s_{11}	Compliance
σ_3	Stress
$E_3(t)$	Electric field
ε_{33}	Dielectric permittivity
B	Magnetic flux density
μ^T	Material permeability
s^H	Elastic compliance under constant magnetic field
λ	Magnetostriction
g	Acceleration
δ	Strain

Chapter 1

Introduction

The new trend technology in electronic devices is miniaturization and lower cost. Although the devices are miniaturized and can be used in diverse areas such as wireless sensors, monitor structural health, can be implanted in human body or can be used in mobile devices, they are still need power. Powering these devices is a significant issue that researchers try to figure out how to disentangle.

Industry and researchers try to find out a way or ways that provide environmental friendly, continuous, and low cost solutions [1]. Energy harvesting refers to capturing energy, which is already available in the environment in different forms and then convert these energy in a useful form for the electronic devices. This energy can be derived from kinetic, solar, thermal or electromagnetic radiation sources [2]. Calio et al. [3] classified the energy harvesting methods as shown in Figure 1.1.Kinetic energy harvesting is one of the most studied method that converting mechanical force or vibration to electrical energy. Several harvesting methods can be employed for the kinetic energy transducer. Electrostatic, electromagnetic, piezoelectric, and magnetostrictive are main energy harvesting methods for mechanical source. Piezoelectric, magnetostrictive energy harvesting techniques consist of smart material that can harness energy based on deformation of these smart materials, however the smart materials are not used for the electrostatic and electromagnetic energy harvesters because these harvesters harness energy by relative motion [4]. The energy transduction for these four types energy harvesting shown in Figure 1.2.

They also emphasized that for motion source, piezoelectric is more efficient in terms

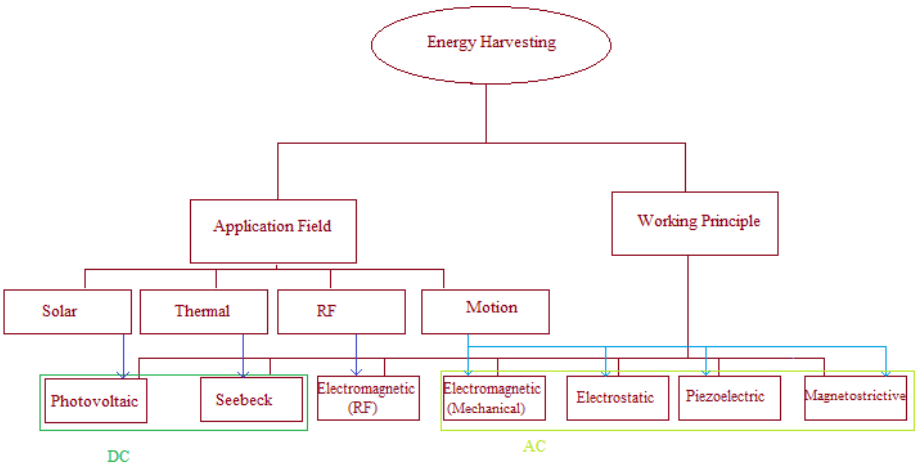

Figure 1.1: Several energy harvesting techniques [3].

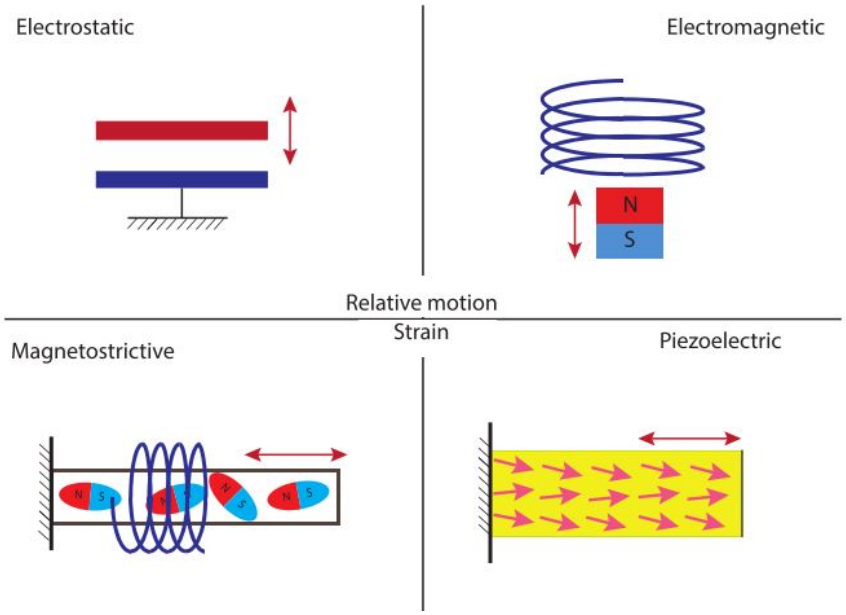

Figure 1.2: Four main kinetic energy harvesting transduction [4].

of power density than electrostatic, which needs initial charge. Also piezoelectric energy harvesting method is more feasible for MEMS applications than electromagnetic ones due the limited miniaturization of magnets in micro scale.

Human motion is one of the most attractive kinetic energy source to harness into useful form. Starner [5] analyzed the human body motion and found that the most promising way to harness energy is from walking. The analysis results are summarized in Figure 1.3 Where the number in the bracket refers to the total power that is produced by each action

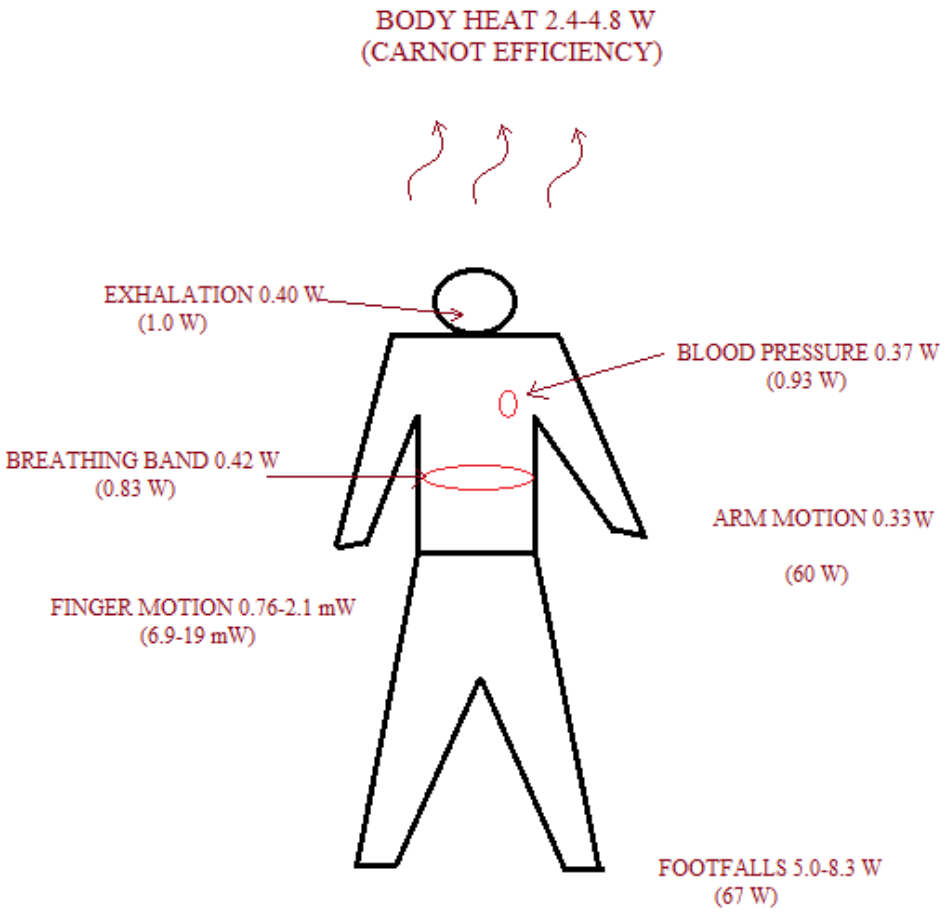

Figure 1.3: Available power from different part of human body; total power for each part is in parentheses [5].

and the outside number refers to amount of power that can be harvested.

Niu et al. [6] stated that although the available power is 67 Watt, which is very high, however, since 70-80% of the energy is stored in the insole, the power that can be obtained is around 2 W. In this research, insole harvesters for human heel have been fabricated by using four different materials to find out the most efficient one in terms of output power. The materials that we will employ are laminated and non-laminated polypropylene (PP), polyvinylidene fluoride PVDF, and one of the magnetostrictive materials- Terfenol-D. The harvesters have been fabricated, tested and then modeled to confirm the results.

1.1 Materials for Harvesters

Piezoelectric polymers are classified into different groups depending on their material structure and physical forms. Simply they are categorized into three groups as shown Figure1.4. The first piezoelectric polymers group is bulk polymers. These polymers are solid films and their molecular structure and orientation provide piezoelectricity. The polyvinylidene fluoride (PVDF) is with a semi-crystalline structure and it is one of the bulk polymers. The second group is piezoelectric composite polymers. The structure of these polymers are combined with piezoelectric ceramics where the piezoelectricity comes from. The third group is voids are introduced and charged polymers and also named cellular polypropylene (PP). The PP film has gas voids and its surface is charged to create dipole, which provides the piezoelectric property. PVDF and PP piezoelectric polymers have been used for insole energy harvester for this study.

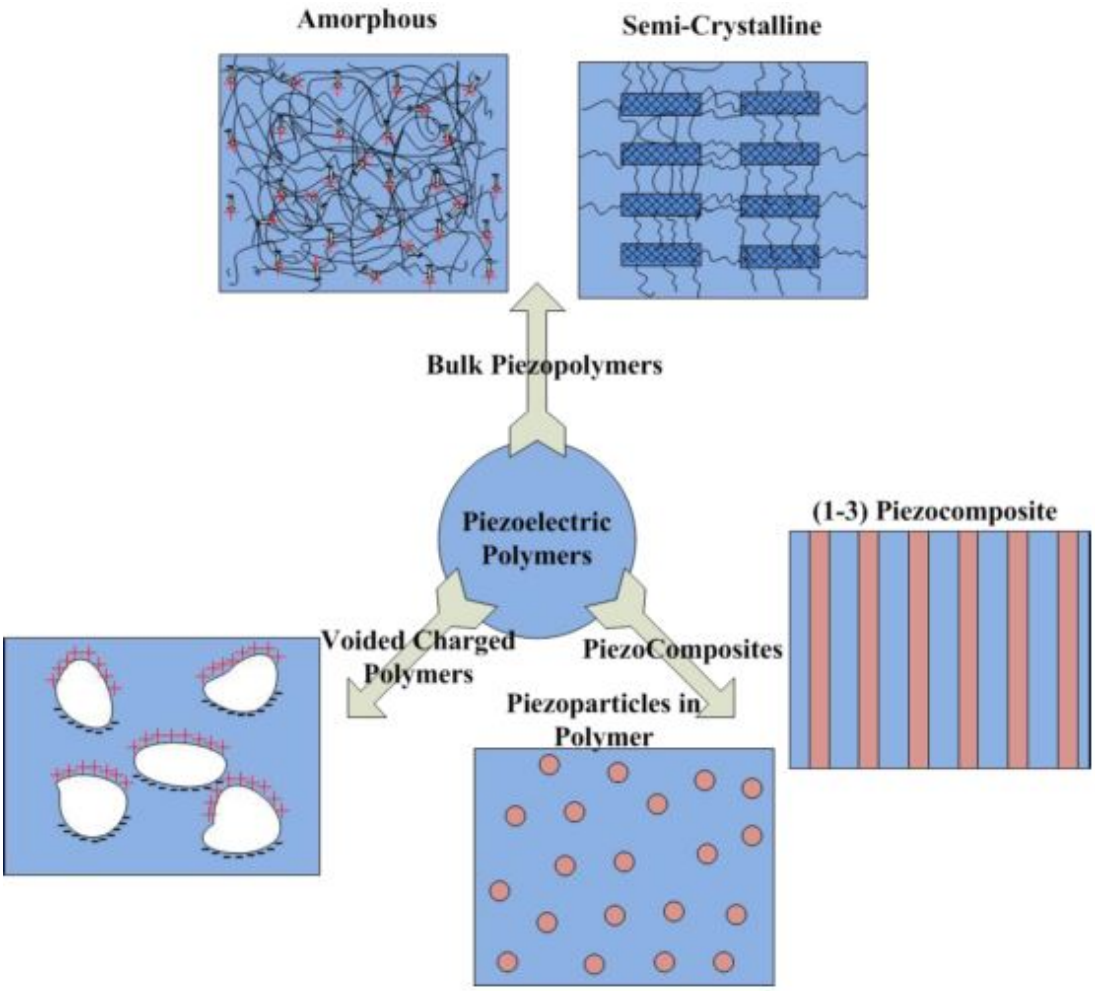

Figure 1.4: Schematic diagrams of piezoelectric polymer categories [7].

1.2 Piezoelectricity

Piezoelectric materials are capable to convert the mechanical energy into electrical energy, meaning that when the material is deformed, this deformation will change charge density on the surface. Therefore, a voltage is produced between the electrodes. It also works inversely meaning that when an electric field is applied to the material, the material will deform, which is called indirect effect while the first one is called direct effect [8]. These piezoelectric effects were first discovered by the Curie brothers in 1880 [7, 9].

There are a couple of piezoelectric coefficients to describe the electromechanical behavior of the piezoelectric materials, which can be derived from each another. The d_{31} and

d_{33} are the most commonly used ones, which are expressed as Coulomb/Newton (C/m^2 per N/m^2) [8]. The first coefficient, d_{31} states that the charges (electric polarization) are produced in a direction vertical to the applied force-stress while the second coefficient, d_{33} indicates that the charges (electric polarization) are produced in the same direction of the applied force-stress as shown in Figure 1.5.

Piezoelectric materials (PVDF polymers and PZT) inherently have special crystal structure and molecules arrangement that piezoelectricity comes from. Therefore, they do not need charge injection. However, since the particles are oriented randomly, there is no net dipole. To produce a net dipole in the polymers, they should be poled under high electric field to reorient the crystals. Unlike PVDF and PZT materials, the PP need to be charged externally. There are several methods for poling: two of them are used commonly: corona and electrode poling [7]. The efficiency of the piezoelectric coefficient (d) depends on a couple of parameters that should be considered during fabrication. These parameters are: the strength and time of the applied electrical field, the value and degree of uniformity of the temperature applied on the polymer and the degree of contamination or voids between the electrodes and the polymer surface [7].

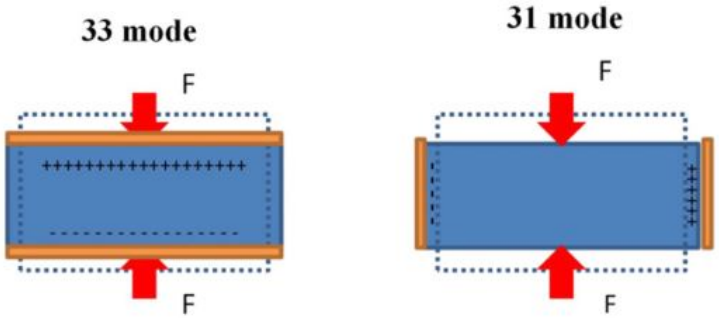

Figure 1.5: Two piezoelectric material d_{31} and d_{33} modes [7].

In order to analyze the behavior of piezoelectric materials, the piezoelectric constitutive equations- developed by Voight [11] are employed in coordination with a single-degree-of-freedom model. The linear constitutive equations for piezoelectric materials are specified in Equation 1.1 and Equation 1.2 [9].

Indirect effect

$$S_3(t) = s_{11}^E \sigma_3(t) + d_{33} E_3(t) \tag{1.1}$$

Direct effect

$$D_3(t) = d_{33} \sigma_3(t) + \varepsilon_{33}^\sigma E_3(t) \tag{1.2}$$

where $S_3(t)$ is the strain, s_{11} is the compliance, σ_3 is the stress, d_{33} is the piezoelectric coupling coefficient, $E_3(t)$ is the electric field, $D_3(t)$ is the electric displacement, ε_{33} is the dielectric permittivity. The first subscript of d_{33} represents the polling direction while the second indicates the loading direction. Equation 1.1 defines the mechanical response of the material while Equation 1.2 defines the electrical response. In this research the loading direction will be 3 because the harvester was tested under compressive force.

Since the harvester is working over a low range of frequencies and also it is assuming that the harvester is subjected to a known stress, the constitutive equations can be simplified using the following relationships:

$$S_3(t) = \frac{x(t)}{L}, \quad \sigma_3(t) = \frac{F(t)}{A_s} \tag{1.3}$$

$$E_3(t) = \frac{v(t)}{h}, \quad D_3(t) = \frac{Q_3(t)}{A} \tag{1.4}$$

where x(t) is the displacement, L is the length of the film, h is the thickness of the film, A_s is the area that is subjected to stress, A is the area of the conductive (electroded) surface, F(t) is the applied force on the film, v(t) is the voltage across to electrodes [9].

1.2.1 Polyvinylidene Fluoride (PVDF)

The challenge in the use of the PZT based piezoelectric materials is due to their mechanical limited capability such as brittleness and difficulties in forming for different applications has forced researchers to find out flexible and higher electromechanical properties materials.

The flexibility and other mechanical properties of PVDF and its copolymers with triflu-

oroethelene (TrFE), tetrefluoroethelene (TFE) and the terpolymers of P(VDF-TrFE-CFE) are the advantages over the PZT ceramics. There are several phases that PVDF possess Without any process PVDF is in α phase, which does not show piezoelectric property. To gain piezoelectric property, PVDF need to be transformed from α to β mechanical orientation, thermal annealing and high voltage treatment have been used to change phase. After transforming the phases, mechanical stretching and poling process need to be applied to induce net dipole [10, 12].

The PVDF is the most studied polymer so far because of its piezoelectric coefficient and flexibility in generating complex designs with less inconvenience and cost. Researchers has focused on the PVDF polymers to increase their piezoelectric properties and the terpolymer of P(VDF-TrFE-CFE) is one of optimized piezoelectric polymers that has high electromechanical properties. The terpolymer, namely relaxor PVDF has been recently developed by Bauer [13]. Terpolymer of P(VDF-TrFE-CFE) is developed by applying proper defect modification in PVDF phase transitions. For detail information about the terpolymers of P(VDF-TrFE-CFE), the reader is referred to [13].

1.3 Ferroelectricity

An electret is a dielectric material that is capable of keeping charges in itself for long time without significant change. Ferroelectret polymers originated from electret. Producing voids inside these polymers and charging these voids create dipoles. When a mechanical force is applied to the ferroelectret polymer, due to the created dipoles, it behaves as piezoelectric material. Ferroelectret film is also called cellular film due to their structure [15].

1.3.1 Cellular Polypropylene (PP)

Several charged foam polymers have been studied such as Polypropylene (PP), Polyethylene terephthalate (PET), Cyclo-olefin copolymer (COC). Cellular polypropylene (PP) is the most studied since it was invented in 1987. The fabrication of the PP includes the following steps: the first step is introducing voids inside the material by injecting micro

scale particles and stretching it; the second step is reshaping the voids by applying gas pressure and heat to increase the piezoelectricity of the PP; and the third step is poling to create dipole. This fabrication process creates anisotropy voids, which are more flexible in thickness direction, (d_{33}) mode. The fabrication process is depicted in Figure 1.6. Upon application of mechanical force or vibration force on PP, the voids' shape will change. Since during PP fabrication process the voids are charged via corona charge or other methods, then any change in voids shape will result in electrical potential difference, which eventually produces charge or voltage [7].

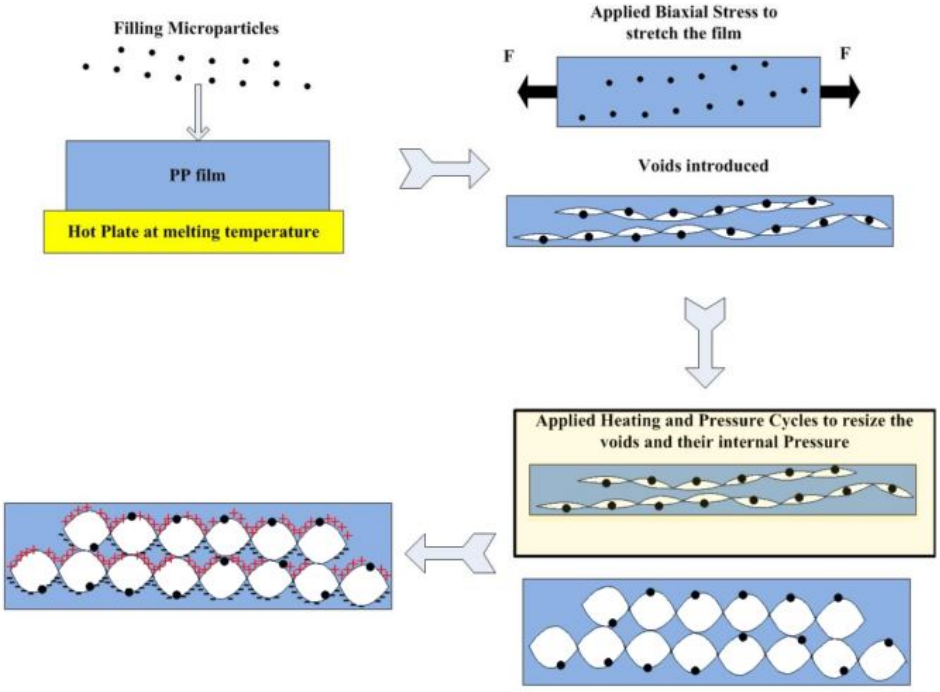

Figure 1.6: The fabrication process of PP [7].

1.4 Magnetostriction

Magnetostriction is property of ferromagnetic materials that undergoes dimension change when expose to the magnetic field or experience magnetization change when a mechanical force is applied. Magnetostrictive materials inherently have magnetic domains, which are randomly oriented before application of any magnetic field. When the magnetic field is applied to these materials, magnetic domains are reoriented and result in dimension

change. Among the magnetostrictive materials, the alloy Terfenol-D is more efficient material in terms of magnestriction. Another alloy is Galfenol (Fe-Ga), which has less magnetostriction than Terfenol-D, however it is more ductile. Metglas is an alloy that has higher piezomagnetic coefficient than Terfenol-D [19].

Magnetostrictive materials have two reverse effects like piezoelectricity. Although nearly all ferroelectric materials have magnetostrictive property, Terfenol-D and other magnetostrictive materials such as Galfenol and Metglas are applicable in terms of these two magnetomechanical effects: Joule effect and Villari effect. Joule effect is when the material experiences a change in shape due to an applied magnetic field, which is known to be used as an actuator. On the other hand, Villari effect is a change in the magnetization when mechanical stress is applied to the material and this effect is known to be used as a sensor. At the same time, Villari effect can also be used in the area of energy harvesting with the help of Faraday's law [16].

1.4.1 Terfenol-D

Terfenol-D is a magnetostrictive material that was developed by Naval Ordinance Laboratory in the United States of America in 1960's. It is made from a combination of rare earth elements: Terbium(Tb) and Dysprosium(Dy), and Iron(Fe) with a chemical composition of $Tb_{0.3}Dy_{0.7}Fe_{1.92}$. It is known to be able to produce high magnetostriction, which can elevate 1600 ppm (part per million) at room temperature and applied magnetic fields strength of 200 kA/m. This high magnetostriction is contributed by the combination of rare earth element, Terbium and Iron. However, this compound is known to have high magnetic anisotropy which reduces the application of the material. To overcome this problem, the addition of Dysprosium at certain amount into the compound is able to reduce the effect of magnetic anisotropy while producing minimal reduction in strain [17].

All magnetostrictive materials are known to have both: Joule effect and Villari effect. For energy harvesting, Villari effect, which is a change in the magnetization when a stress is induced in the material, is considered. This conversion of energy is represented by linear

equation of state,

$$B = \mu^T H + d\sigma \tag{1.5}$$

$$S = dH + s^H \sigma \tag{1.6}$$

where B is the magnetic flux density, d is the linear coupling coefficient, σ is the induced stress, μ^T is the material permeability under constant stress, H is the magnetic field strength, s^H is the elastic compliance under constant magnetic field, and S is the strain in thickness direction [16, 19]. The produced magnetic flux density is picked up by a pick-up coil which in turns produce output voltage as per Faraday's Law, induced voltage across the terminal is

$$V(t) = NA\frac{dB}{dt} \tag{1.7}$$

where N is the number of coil's turns and A is the cross-sectional area of coils.

To increase the effectiveness of using Terfenol-D composite, Rodriguez et al. [20] showed that aligning the Terfenol-D particles during curing can increase the magnetostriction (λ) of the material [18, 20].

1.5 Literature Review

This section will review literature on insole energy harvesters.

1.5.1 Piezoelectric Harvesters

Several types of structures have been employed for piezoelectric shoe harvester. Each structure proposed different shapes and elements to maximize the power generated. Xin et al. [22] classified structures used in shoe harvester into: flat plate, arch and cantilever, as shown in Figure 1.7.

Rocha et al. [23] designed a combined power harvester with polyvinylidene fluoride (PVDF) and electrostatic transducers to increase output power. Since electrostatic har-

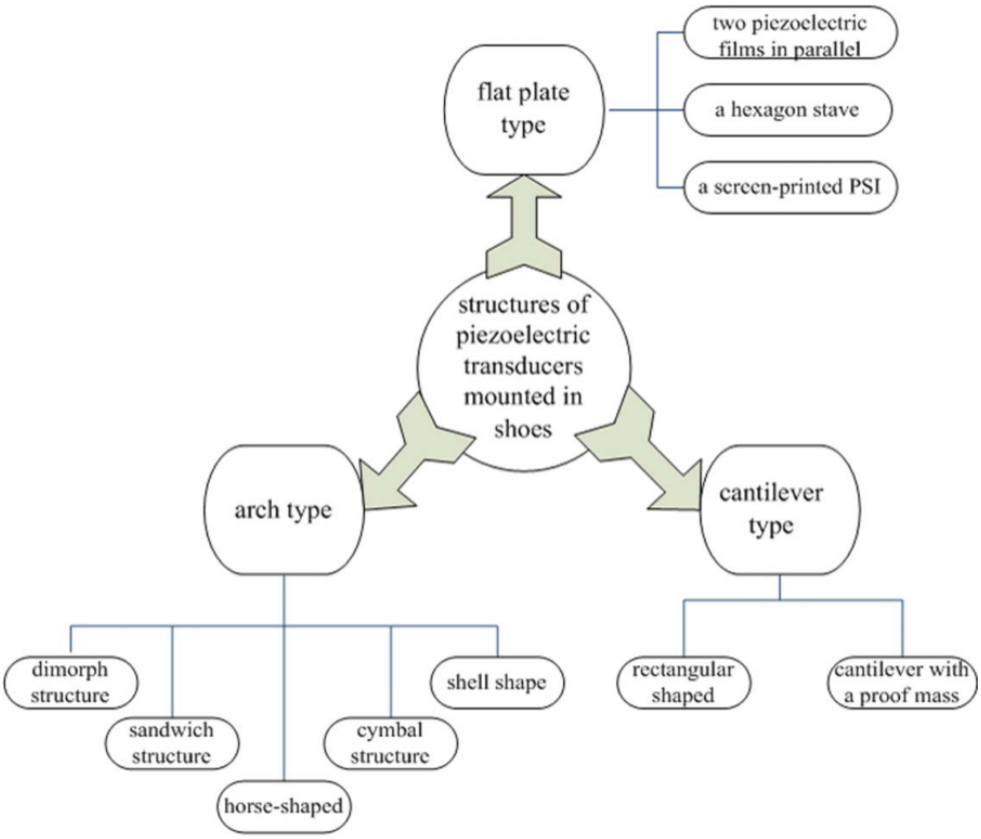

Figure 1.7: Different design for shoes harvester [22].

vesters need initial charge, PVDF behaves as an initial charger. The experimental results show that the output power of combined harvester is greater than that of PVDF alone.

Shenck [21] indicates that d_{31} conversion mode is more efficient than other modes due to material properties even though human weight compresses the material in d_{33} mode. His group explored two approaches for d_{31} mode energy harvesting from human walking. The first one is designed to take advantage of bending of the ball of the foot to induce current. To make sure that the design will not discomfort the foot, the group used PVDF, which is flexible. The design adopts a sandwich structure with each side having eight layers of PVDF films. The second one is made of semi-flexible piezoelectric lead zirconate titanate (PZT) that is laminated with spring metal strip. This structure is proposed to capture energy from heel strike. The average output power for the PVDF harvester, delivered across a 250 kΩ load resistor at a 0.9-Hz walking pace was 1.3 mW while the PZT dimorph's average output power was 8.4 mW delivered across a 500 kΩ load resistor

when a similar force was applied.

Niu et al. [6] analyzed the possibility of power generation from different parts of the human body such as joints (ankle, knee, hip, shoulder, and elbow), heel strike, and whole body center mass locomotion. They showed that previous studies overestimated available input power, therefore they proposed different estimation technique to calculate the power that can be harvested from human kinetic energy. They report that the power available at heel strike is 2 W.

Zhao [24] designed two PVDF shoe energy harvesters: under heel only or the heel and forefoot. The PVDF films were sandwiched between two wavy structures to maximize energy conversion via d_{31} mode. The average output power was 1 mW in the first prototype and 90 μW for the heel and 30 μW for the forefoot in the second prototype.

Another shoe harvester was designed by Fourie [29] to generate power from heel strike. The harvester was designed in horseshoe shape and includes fifteen PVDF films, where each is placed vertically between two plates. Each unit includes 52 μm thick and 12.7 mm tall PVDF film on PET plastic substrate. The PET substrate behaves as spring.

1.5.2 Ferroelectric Harvesters

Since piezoelectric foam (PP) is leads free, it has an advantage over PZT based ceramics while it has limited thermal stability. A summary comparison of piezoelectric foam with PVDF, conventional PZT, and single-crystal lead magnesium niobate-lead zirconate titanate (PMN-PZT) is given in reference [28]. Piezoelectric constant (pC/N) for piezoelectric foam and PVDF were given 25-250 (d_{33}) and -33 (d_{33}), respectively.

Luo et al. [30] conducted several researches on cellular polypropylene (PP) for energy harvesting. In the first study, they designed a single and a multilayer PP harvesters in the size of 60$\times$ 70 mm for mode d_{33}, meaning it is tested under compressive force. The harvesters were tested under three different walking modes: slow, normal, and fast walking mode. According to their analysis, since the momentum would change under different walking mode, the output voltage would also change. The higher momentum would produce higher voltage in positive peak and negligible change in negative peak [30].

Therefore, they indicated that at speed walking, the output power would be higher. The single layer produced 10.2 μW and the ten layers harvester produced 100 μW with 1 MΩ load at normal walking mode. In another study, they built several harvesters, which had different number of layers:10, 20, 30, 40, 80 produced 19.8 μJ, 31.9 μJ, 40.2 μJ and 65.6 μJ, respectively [31].

Ray et al. [32] studied multilayer PP harvester that is tested under harmonic base excitation. The output power was 0.45 μW for 20-layer harvester in 20 minutes while it was 0.89 μW for 40-layer when it is excited at 0.5 g acceleration. They also proposed an electromechanical model for their harvester.

1.5.3 Magnetostrictive Harvesters

The usage of Terfenol-D as energy harvester has been studied since early 2000's. Staley et al. [33] used a Terfenol-D and Galfenol rods that was wrapped with pick-up coil and attached to a simply supported beam with a mass at one end of the beam. The device was placed on a shaker where the vibration caused by the shaker will vibrate the beam and consequently pressing the rods to produce magnetic field.

Besides using rod, a sheet of magnetostrictive material was used to harvest energy. Wang [34] used Metglas, an amorphous metallic glass to generate magnetic field. The Metglas sheet was attached to a copper sheet and placed into pick-up coil. One end of the attached sheet was fixed to a shaker and the other end was left free. The vibration from the shaker shook the sheets and consequently generating magnetic field that was picked-up by the coil.

However, the study of using Terfenol-D particles as energy harvester is still new. Currently, the usage of Terfenol-D particles is only being used as an actuator where it is mixed with polymer resin, such as polyurethane (PU). The purpose of making the composite is to reduce the effect of eddy current at high frequency and to overcome the issue of brittleness of Terfenol-D during operation [20, 36].

1.6 Objective

The objective of this thesis is to develop an insole energy harvester to power a designated electronic device with or without a battery. For that purpose four different materials have been employed that include the non-laminated polypropylene and laminated propylene (PP), polyvinylidene fluoride (PVDF), and a magnetostrictive material, namely Terfenol-D. The first three piezoelectric polymers are commercially available and purchased. The Terfenol-D was suppled as powder, therefore it needs to be processed to as rough material. In order to gain piezoelectric property, it needs fabrication processes that includes combining with polymer and poling. The purpose of using these materials is to find out the more efficient one that meets our needs.

After fabricating the harvesters by using simple and repeatable fabrication process, test these harvesters to find out the efficient one that higher output power.

Chapter 2

Fabrication of Harvesters

2.1 PVDF and PP

The terpolymer of P(VDF-TrFE-CFE) was purchased from Piézotech S.A.S. The size of the film was 12×12 cm with 40 μm thickness with laminated Cr/Au electrodes. Laminated and non-laminated polypropylene (PP) films were purchased from the EMFIT (Emfitech Ltd, Finland) as 60×90 cm sheets with 120 μm and 85 μm thickness, respectively. Both PP were supplied without electrodes.

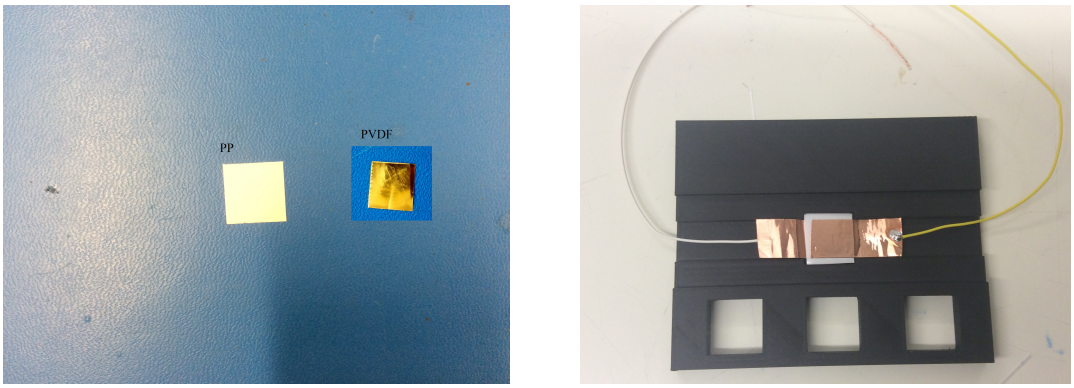

(a) Film samples. (b) Individual harvester units.

Figure 2.1: Fabrication of harvester units.

The films was cut into 1×1 cm for the first harvester prototype. The output power was low, so the sample size was increased to 1.6×1.6 cm to improve the reliability of the experiments After cutting the samples to size, Figure 2.1a, 3M EMI conductive adhesive

copper tape electrodes were attached to each sample, Figure 2.1b.

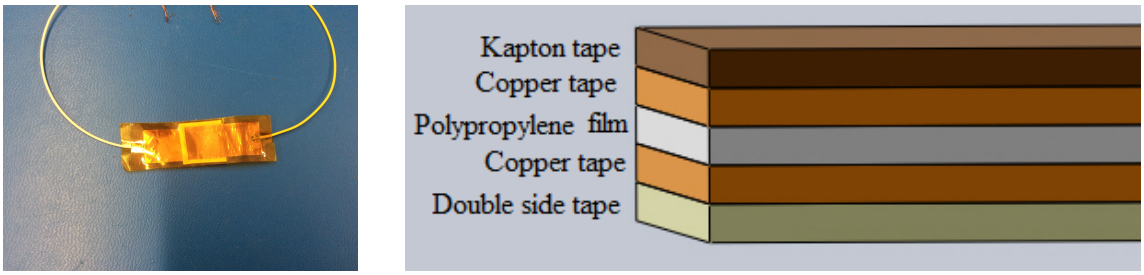

(a) Insulated film sample. (b) Structure of one unit (layer) harvester.

Figure 2.2: Fabrication of full harvester prototypes.

In order to prevent short circuits, each harvester unit were insulated with 3M kapton tape, Figure 2.2a. The individual harvester units were bonded together using 3M double sided tape. The overall structure of the harvester prototypes is shown in Figure 2.2b. Bonding harvesters is important to synchronize the stress distribution and charge generation in each layer. The layers, harvester units, can be connected electrically in parallel or in series. IN our case, we connected the harvesters in parallel to increase output current.

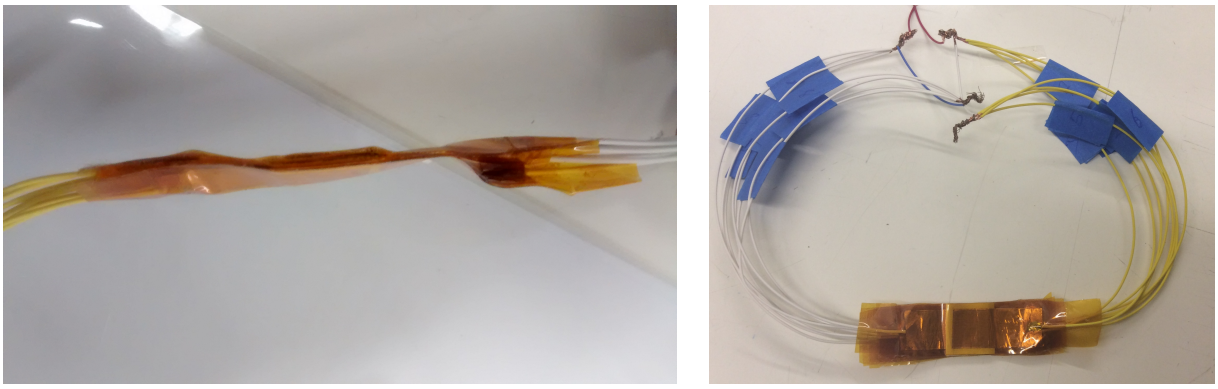

(a) Side view of eight layers PP harvester. (b) Top view of eight layers PP harvester.

Figure 2.3: Harvester prototypes.

The fabrication process of the non-laminated and laminated Polypropylene (PP) were performed with terpolymers of P(VDF-TrFE-CFE) as explained above. After bonding eight harvester units, Figure 2.3, the total thickness for PVDF, non-laminated, and laminated (PP) was measured as 2.30 mm, 2.40, and 2.50 mm, respectively.

2.2 Terfenol-D

Terfenol-D particles with the size of 250 - 300 μm was supplied by ETREMA and two-component low hardness polyurethane (PU) resin (Smooth-Cast 60A) was supplied by Smooth-On, Inc. PU was used as a matrix to embed Terfenol-D particles. The low hardness PU was used in consideration of shoe wear comfort when the composite is placed in shoe heel.

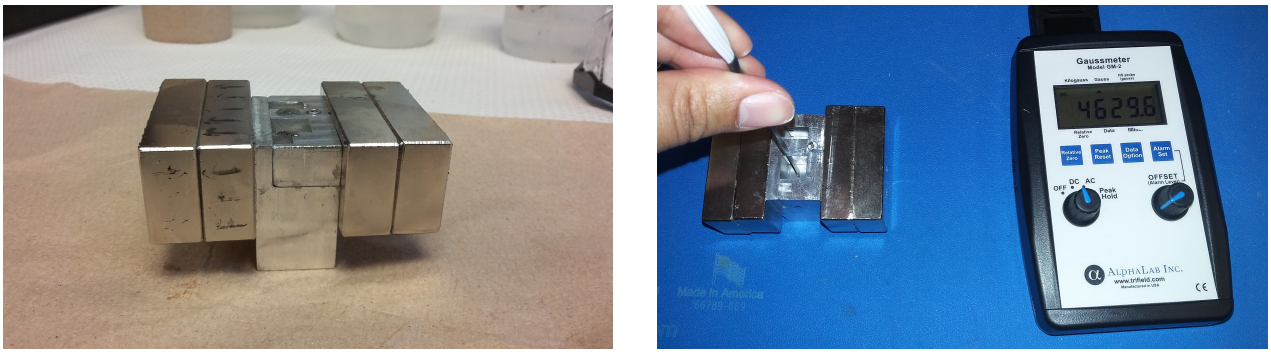

(a) Permanent magnets attached to mold sides. (b) Measuring the stength of magnetic field.

Figure 2.4: Methodology for Terfenol-D composite fabrication.

An aluminum mold with a cavity size of 1 x 1 x 1 cm was prepared to allow the composite to harden after mixing. To ensure the composite would not be too hard, Terfenol-D particles ration in the mixture was limited to 20 wt%. The addition of Terfenol-D particle was done after the two components of PU resin were combined together for 10 minutes to ensure full reaction of the components. Then, the mixture was poured into the mold and a magnetic field density of 0.45 T was introduced to align the particles in the composite as depicted in Figure 2.4a. The magnetic field strength was measured using a Gaussmeter as shown in Figure 2.4b. The mold was placed in a furnace to cure at a temperature of 80 ℃ for 24 hours to remove any moisture from the composite.

Figure 2.5a show three different size cured samples of Terfenol-D composite, $1 \times 1 \times 0.5$ cm, $1 \times 1 \times 1$ cm, and $1 \times 0.5 \times 0.5$ cm. After curing, the composite was wrapped with 100 turns of 30 AWG copper wire perpendicular to the particle alignment direction. The wire wounded Terfenol-D composite is shown in Figure 2.5b.

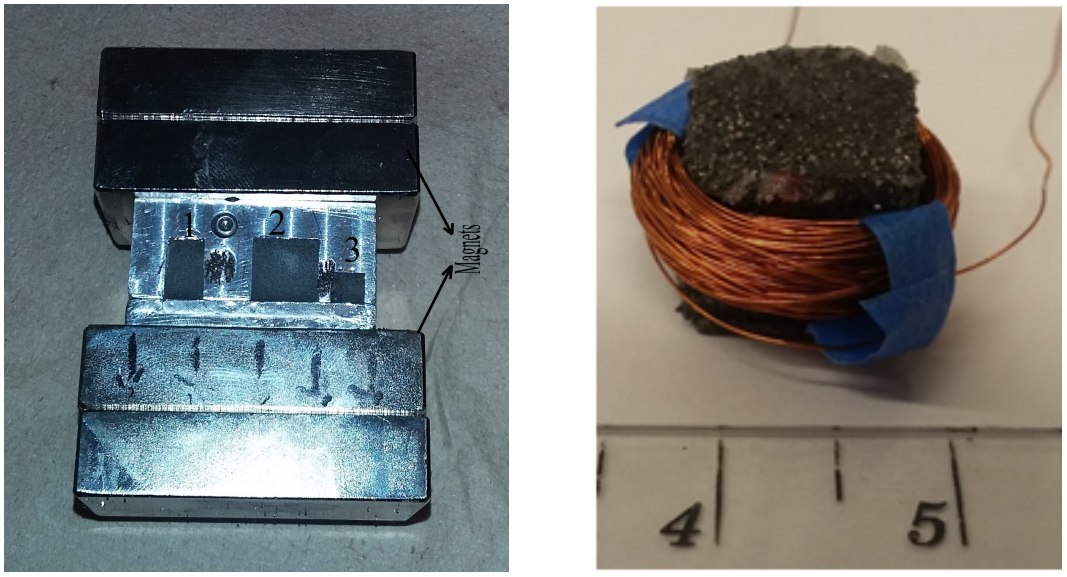

(a) Three different Terfenol-D sample sizes in mold.

(b) Terfenol-D harvester.

Figure 2.5: Terfenol-D composite harvesters.

Chapter 3

Electromechanical Model and Power Management

3.1 Model

A harvester unit model as shown in Figure 3.1 was studied. The applied force (F) is in compressive mode, namely d_{33} mode and the voltage($V_{out}C_p$) exists between top and bottom electrode.

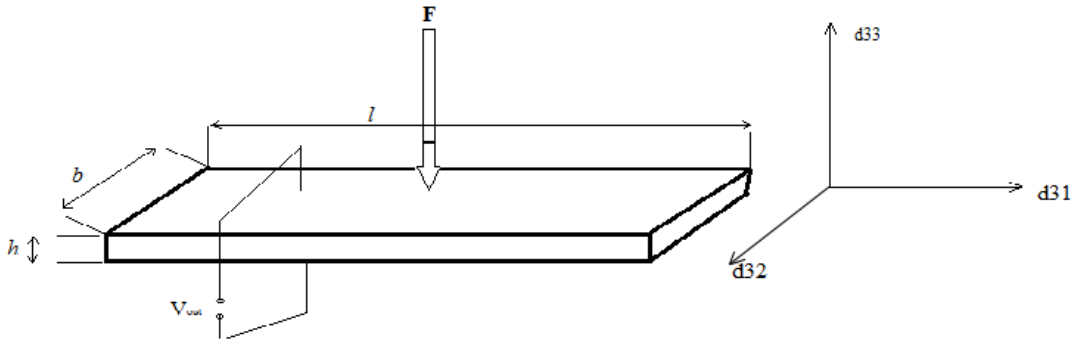

Figure 3.1: A capacitor model for ferroelectret. [27].

As discussed in Section 1.2, the piezoelectric constitutive equations were used to describe the behavior of piezoelectric materials when exposed to mechanical or electrical fields. These equations are the basis for the calculation of produced charge. The model

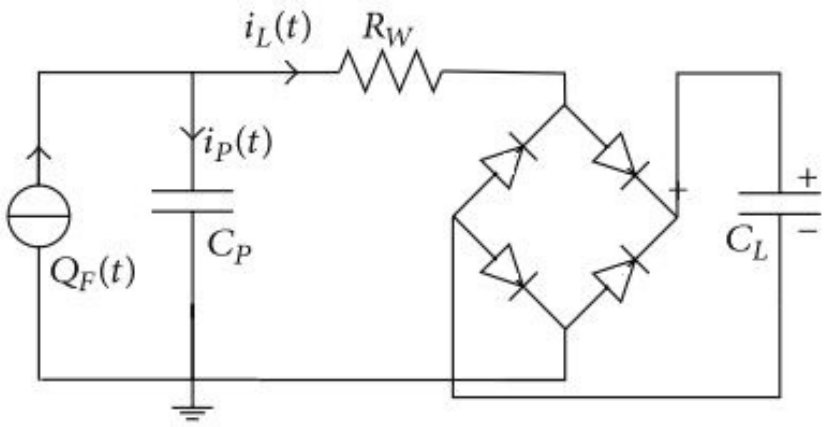

Figure 3.2: Electric circuit diagram of the energy storage model. [26].

to calculate energy and power is based on the electromechanical model developed by Zhao [26].

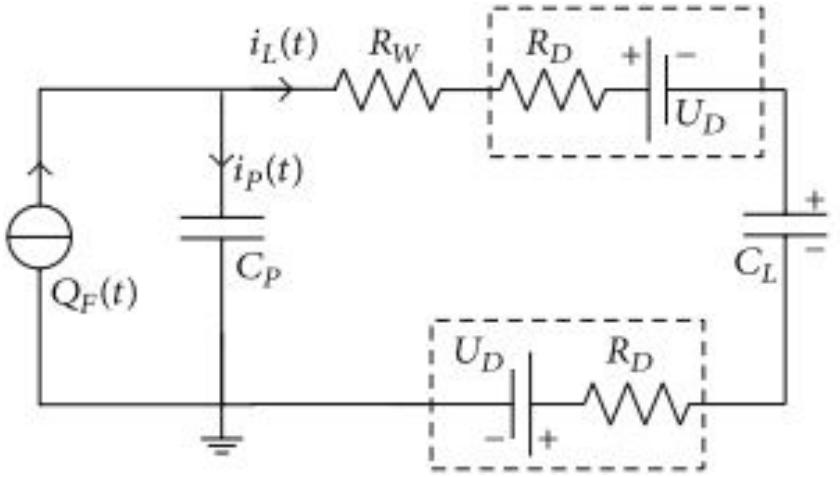

Figure 3.3: Schematic of the circuit when diodes are active[26].

They proposed three models: resistive load model, capacitive load model, and energy storage model. In this research, the storage model used to calculate charges and stored energy. The energy storage model circuits with a unit harvester are shown in Figures 3.2 and 3.3 where C_p is the unit harvester capacitor, C_L is the storage capacitor in the circuit, U_D is the voltage across each diode in the bridge rectifier and it assumed as 0.5 V, R_w is the wire resistance and it is ignored in the model because it is small and R_D is the diode resistance.

Charge density on the surface when the force is applied is given by:

$$D_3(t) = \frac{Q_3(t)}{A} \tag{3.1}$$

Applied stress on the harvester is given by:

$$\sigma_3(t) = \frac{F}{l \times b} \tag{3.2}$$

The total produced charge is given by:

$$Q_F(t) = N d_{33} \sigma_3 A = Q_3 + V_{out} C_p \tag{3.3}$$

where F is the applied force, l is the length, b is the width of the harvester, h is the thickness of film, A is the electrode area, $V_{out}(t)$ is the output voltage, $Q_3(t)$ is the total charges accumulated on the electrodes, C_p is the capacitance of harvester unit, and N is the number of film layers in harvester. Since C_p is much smaller than C_L, $V_{out}C_p$ is negligible; therefore, the produced charge by force is

$$Q_F(t) = N d_{33} \sigma_3 A \tag{3.4}$$

The energy stored in the load capacitor when the force is applied to the harvester is given by:

$$E = \frac{1}{2} C_L V_{out}^2 \tag{3.5}$$

This model considers that the charges are drained from the harvester in two cases for each cycle; when the force compress the harvester and when the force is removed. In these two case, charges will go through the diodes and stored in the load capacitor. In order to calculate the charges that are stored in the load capacitor, a few assumptions and

simplifications have been done. These simplifications are listed in the following equations:

$$a_1 = \frac{C_L}{C_L + C_P} \tag{3.6}$$

$$a_2 = \frac{C_P}{C_L + C_P} \tag{3.7}$$

$$b_1 = (a_1 - a_2)a_1 \tag{3.8}$$

$$b_2 = (t_2 - t_1)t_2 \tag{3.9}$$

$$b_3 = b_1 + b_2 = (a_1 - a_2)^2 \tag{3.10}$$

$$c_1 = -4a_1^2 U_D C_P - 2a_1 U_D C_P + 2a_1^2 Q_F \tag{3.11}$$

$$c_2 = 4a_1 a_2 U_D C_P - 2a_1 U_D C_P - 2a_1 a_2 Q_F \tag{3.12}$$

$$c_3 = 2Q_F(a_1 - a_2)a_1 - 8a_1^2 U_D C_P \tag{3.13}$$

After these simplifications, the total charge on the load capacitor is calculated in Equation 3.14

$$Q_L(t) = \frac{b_1 c_3}{b_3 - 1}(b_3)^{(t-1)} - \frac{b_1 c_3}{b_3 - 1} + c_1 \tag{3.14}$$

The total generated energy stored in the load capacitor for the model is

$$E = \frac{Q_L(t)^2}{2C_L} \tag{3.15}$$

The maximum output power of the harvester that is delivered to the capacitor is:

$$P_{mx} = \frac{dE}{dt} \tag{3.16}$$

Average output power of the harvester that is delivered to to the capacitor is given by

$$P_{av}\frac{\Delta E}{\Delta t} \tag{3.17}$$

The power that is dissipated by the resistor load (R_L) of the harvester is

$$P = \frac{{V_{rms}}^2}{R_L} \tag{3.18}$$

3.2 Quantifying Force

Many researches have been done to analyze and model the human motion. These researches are important because they provides solutions for different problems including of the health and industrial aspects. Analysis of human motion is significant parameter to predict available energy that can be converted. In their study, Niu et al. [6] indicated that once the heel touches the ground, it will compress the insole and around 4-5 cm displacement will exist. However, due to the elasticity of the insole, some of that energy will be stored and only the rest of energy will be available to capture and generate electricity by the energy harvester.

When we tested the harvester we tried to imitate the human walking. The frequency of human walking is around 1 Hz, however since we tested the harvester by the shaker and due to the limitation of the setup, at least 10 Hz was applied because when the frequency increased, the feedback from accelerometer caused an error. Since the heel size area is around 40-46 cm^2 [24, 25] and we considered human a mass of 80 kg, the stress on the 46 cm^2 heel size will be around 174 kPa. In this research the harvester size was tried to keep small as possible as it could be. The final harvester size was 1.6 $\times$1.6 cm which corresponds to 2.56 cm^2 area. For this area 44.5 N was supposed to be applied to resemble the force from human walking, however the force that shaker provided was 5.9 N at 1 g and 10.6 N at 1.8 g accelerations. Related calculations are in the following equations;

The stress that is applied on the human heel with 80 kg mass is

$$Pr = \frac{800}{46 \times 10^{-}4} = 174\,\text{kPa} \tag{3.19}$$

The period of human walking is

$$T_h \geq 1\,s \tag{3.20}$$

The available power from the heel strike is

$$P = \frac{\Delta W}{\Delta t} = \frac{F_h \delta}{T_h} \leq 800\delta\,\text{W} \tag{3.21}$$

The harvester size is

$$A_h = 1.6 \times 1.6 = 2.56\,cm^2 \tag{3.22}$$

The force that supposed to be applied to the harvester is

$$F_h = Pr\,A_h = 44.5\,\text{N} \tag{3.23}$$

The shaker period is

$$T_p = 0.1\,s \tag{3.24}$$

Power input that was supposed to be provided by the shaker is

$$P = \frac{\Delta W}{\Delta t} = \frac{F_p \delta}{T_p} = 445\delta\,\text{W} \tag{3.25}$$

The force that is applied to the harvester during test at 1 g acceleration is

$$F_{h1} = 5.9\,\mathrm{N} \tag{3.26}$$

The actual power supplied from the shaker is

$$P = \frac{\Delta W}{\Delta t} = \frac{F_p \delta}{T_p} = 59\delta\,\mathrm{W} \tag{3.27}$$

where δ is the strain and the force F_{h1} was measured by FSR 406 force sensor is shown in Figure 3.4 when the shaker was excited at 1 g acceleration. During the force measurement, the force sensor was placed under the harvester.

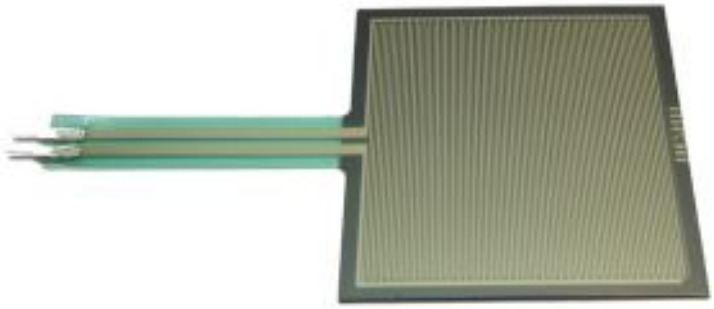

Figure 3.4: Force sensor FSR 406 [39].

3.3 Power Management Circuit

Since piezoelectric harvester provides high AC voltage and low current, the output of the harvester needs to be rectified because without rectification, the output power of harvester is not useful to power most of the electronic devices. In order to convert the AC voltage to DC form rectifier circuit is employed. Depending on the application, different techniques with different components can be employed to condition the power. Mostly, full-wave bridge is employed in a power management circuit to convert the AC power to DC. The power management includes a capacitor to store the output energy and also to smooth the input voltage when it is not in use [24].

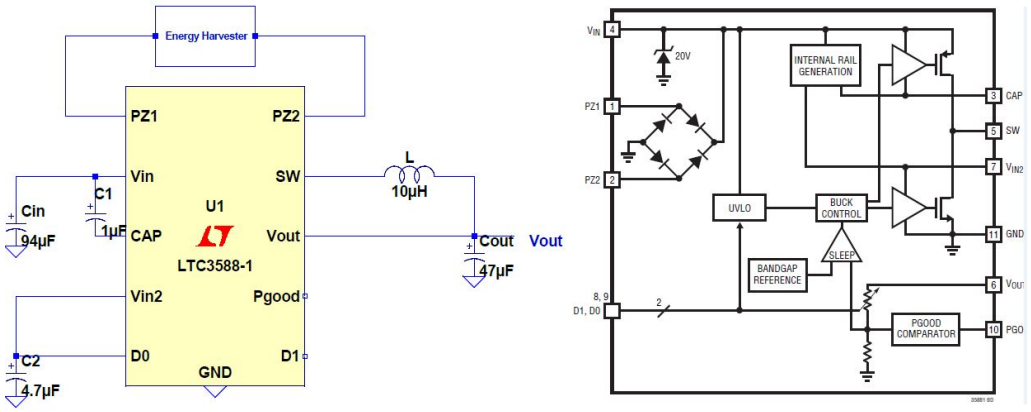

Figure 3.5: Electrical circuit and block diagram of the LTC3588-1 [38]

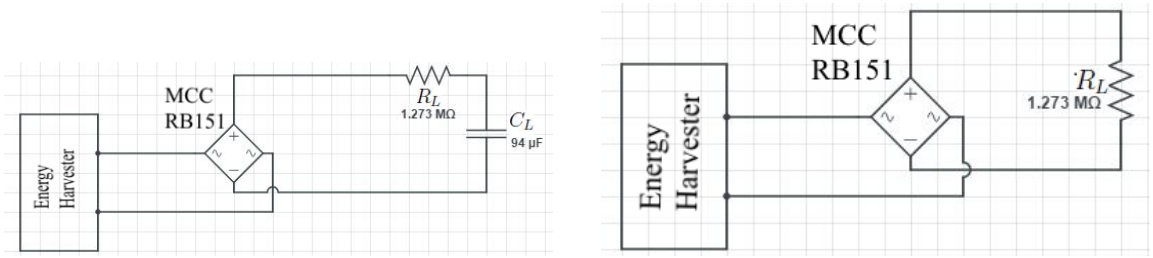

Figure 3.6: Harvester electrical circuit diagram with the full-wave bridge rectifier a) with resistive (R_L) and capacitive load (C_L) and b) with only resistive load (R_L).

In this research, initially, the LTC3588-1 power management integrated circuit was used to rectify power. The electrical circuit and block diagrams of the LTC3588-1 are shown in Figure 3.5. The LTC3588-1 includes a full-wave rectifier and a a buck converter to control the stored energy. At first, generated energy is stored in the input capacitor C_{in} and when the voltage across to the input capacitor C_{in} reaches the threshold voltage, the buck converter is activated and then the energy is transferred to the output capacitor C_{out}. The LTC3588-1 integrated circuit allows to select different output voltage ranging from 1.8 V to 3.6 V. In our case the output voltage was set to 2 V. Once the output voltage attains 2 V, the load was powered [38]. For the LTC3588-1 integrated circuit, the input capacitor C_{in} is 94 μF and output capacitor C_{out} is 47 μF.

Experimental results showed that the output power of the LTC3588-1 integrated circuit is excessively low compared to the power dissipated by the resistive load. Then different rectifiers were employed. The output power was measured with full-wave silicon diode

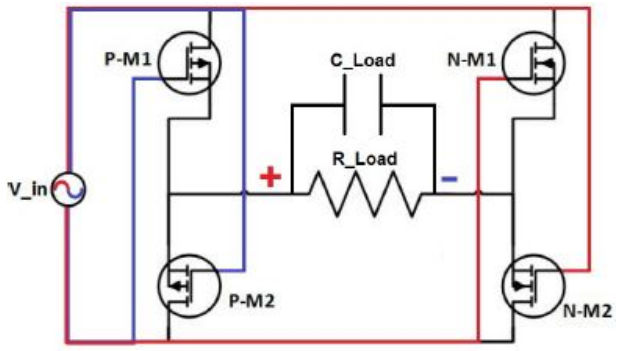

Figure 3.7: Schematic diagram of MOSFET ful-wave rectifier [37]

bridge rectifier MCC RB151 in two different circuit configurations: first the power delivered to the load (R_L) was measured and then the capacitive load (C_L) was added and the energy stored in the capacitor was calculated. These two circuits are shown in Figure 3.6.

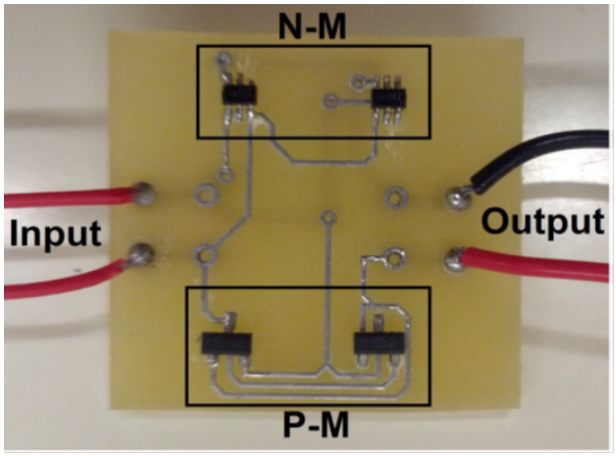

Figure 3.8: Picture of the fabricated full-wave bridge rectifier [37]

Then another full-wave bridge rectifier, which was designed in our lab, was utilized. Four MOSFET transistors, two P-channel and two N-channel, were employed for this circuit as shown in Figure 3.7. This circuit was fabricated on PCB as shown in Figure 3.8. P-M1 and N-M2 conduct current during positive peak input voltage, however P-M2 and N-M1 are in cutoff mode. P-M2 and N-M1 conduct current during negative peak input voltage while P-M1 and N-M2 are in cutoff mode [37]. Since this rectifier was designed for electromagnetic energy harvester, it requires low voltage and high current, which is opposite to the piezoelectric energy harvester that produces high voltage and low current. Consequently this full-wave bridge rectifier did not work for our case.

Chapter 4

Experiments and Results

4.1 Experimental Procedure

The aim of the experiments was to evaluate the performance of the harvesters designed and fabricated in Chapter 2. Towards that end, we measured the open-circuit voltage of those harvesters as well as the output power they delivered to different external loads under various input force profiles.

The test setup built for these experiments is shown in Figure 4.1. An electromagnetic shaker, Labworks Inc.'s ET-126-1, was used to deliver acceleration to a brass rod with a known mass ($m = 0.255\,\text{kg}$) acting as a hammer. The shaker was driven using Labworks Inc.'s Pa 138 power amplifier. A controller, Vibrayion Research's VR9500 Revolution, was used to command and maintain the desired acceleration amplitude and frequency via closed loop control. Output voltage was measured and stored digitally through Tektronix TDC2004C oscilloscope.

The shaker was fixed to the table. The hammer (brass rod) was attached to the shaker as a moving mass. A metal block was used as stopper to hold the harvester in front of the hammer. The harvester was tapped into the block aligned with the hammer. Once the shaker is actuated, the hammer impacts the harvester delivering a periodic force. Due to the limitation on the shaker stroke size, the minimum excitation frequency was set to 10 Hz. The frequency and acceleration magnitudes were commanded via the controller interface, Vibrayion Research's 'Vibration VIEW 9', shown in Figure 4.2.

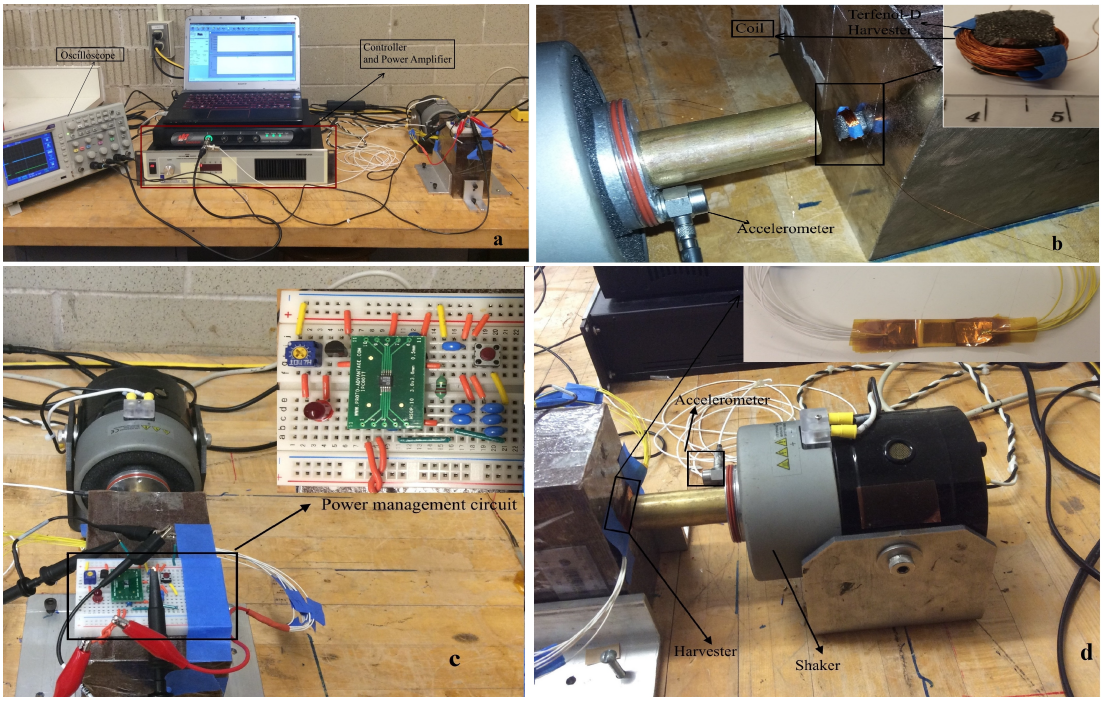

Figure 4.1: Experimental setup a) General setup view, b) Terfenol-D harvester, c) Power management circuit including LTC3588-1, d) PP harvester is attached to th block across the shaker.

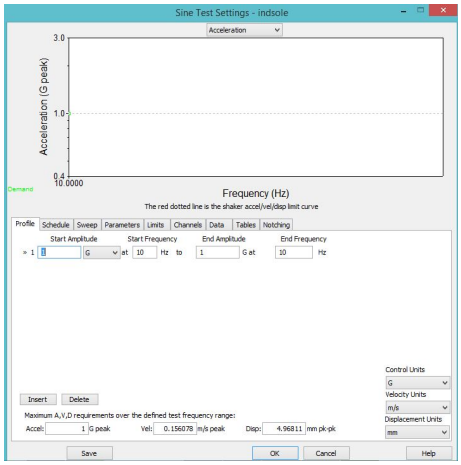

Figure 4.2: Controller interface

Figure a is a general view of the experimental test setup and Figure b shows the Terfenol-D harvester test setup- wire wound Terfenol-D is attached to the metal block, The electrical circuit on the top of the block is shown in Figure c and Figure d shows the 8-layer PP harvester that is attached to the metal block.

4.2 Ferrolectric Harvesters

Firstly, the power that is delivered by the resistive load was calculated with different values of the resistors to find out the optimal power that matches with the harvester impedance as shown in Table 4.1. As it is shown in Figure 4.3, when power reaches to a certain point, the power decreases due to ohmic loses. The resistor value that delivers maximum power value is the optimal resistor for the harvester. The optimal power that is dissipated on the resistive load was 617 μW that was calculated using Equation 4.1, where optimal resistance load R_L was 1.273 MΩ and the RMS voltage V_{rms} was 28 V when sinusoidal force was applied at 2 g acceleration. The RMS voltage was calculated by the average root mean square formula given by Equation 4.2 by processing the data (the output voltage of the harvester) that was saved by the oscilloscope where V_i^2 is the discretized voltage and N is the sample number [37]. The optimal power and RMS voltage V_{rms} are depicted in Figure 4.3.

$$P = \frac{V_{rms}^2}{R_L} \tag{4.1}$$

$$V_{rms} = \sqrt{\frac{\sum_i V_i^2}{N}} \tag{4.2}$$

When the force was applied at 2 g acceleration the controller gave errors thus the acceleration of the shaker was decreased and applied the force at 1.8 g acceleration for setup safety. Therefore, it is obvious that when the force changes, the output power would change due to the fact that the produced charges are proportional to the force. The maximum output power delivered to R_L = 1.273 MΩ was 240 μW when the force was applied at 1 g acceleration and it was 516 μW (Equation 4.2 was used to calculate power) at 1.8 g acceleration where the force at 1 g and 1.8 g accelerations correspond to 5.9 N and 10.6 N (kg.m/s^2), respectively.

Then the conditioned output power of the LTC3588-1 integrated circuit was calculated.

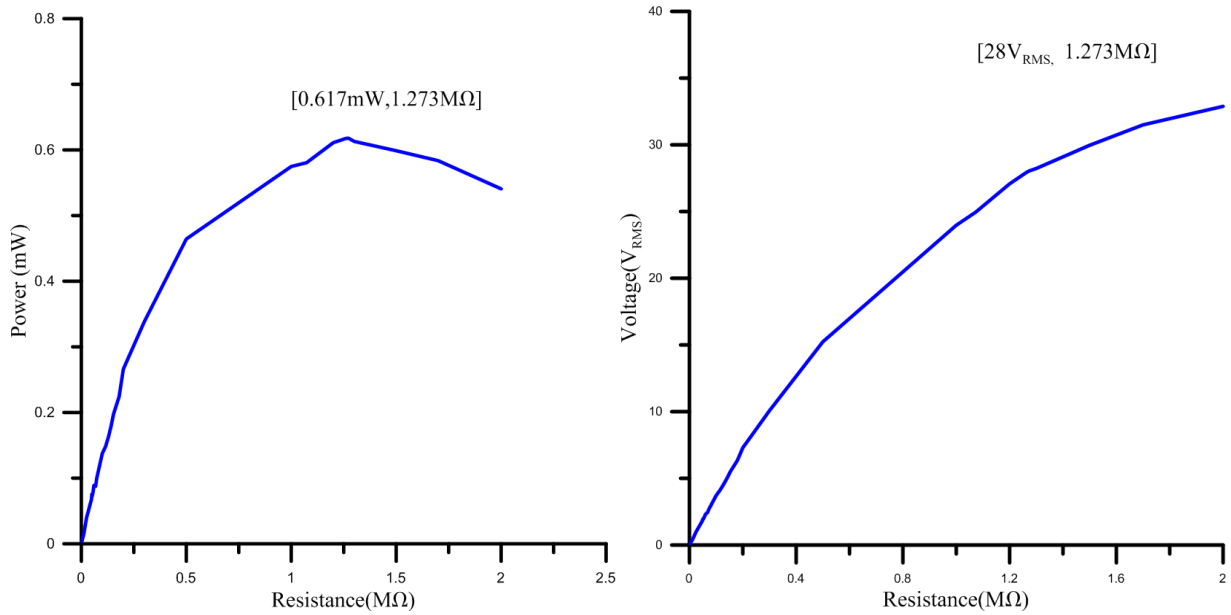

(a) Output power as a function of resistive load for PP.

(b) V_{rms} as a function of resistive load for PP.

Figure 4.3: Optimal power and V_{rms} across the resistive load.

The input capacitor load was C_{in}=94 μF and output capacitor was C_{out}=47 μF. The maximum output power of the LTC3588-1 integrated circuit as calculated in Equation 4.5 was 19 μW when the force was applied at 1.8 g acceleration while it was 14.4 μW at 1 g acceleration.

Figure 4.4a shows the output voltage of LTC3588-1. C_{in}=94 μF took 95 seconds to reach 4 V and once the voltage (V_{in})on the input capacitor reached 4 V, buck converter was activated and the energy was transfered to the output capacitor C_{out}=47 μF. Since the output capacitor was set to 2 V, at 2 V external load (LED) was powered for 2-3 seconds. After LED was powered ON, voltage on the capacitors decreased to a certain level then after 20 seconds the voltage reached to threshold level again and LED was powered ON. This cycle is repeated every 20 seconds as long as the shaker was excited. The rectified output voltages of the PP harvester using LTC3588-1 with capacitive load and without

Table 4.1: Non-laminated PP harvester output voltage and power as function of resistive load R_L).

.

Resistive load R_L (kΩ)	RMS voltage (V)	RMS Power (μW)
3	0.1	4
50	1.9	75.7
73	2.7	96.6
100	3.7	138
141	51	178
200	7.3	266
300	10	338
500	15.2	464
1000	24	575
1200	27	611
1260	27.85	616
1273	28	617
1300	28.2	613
1500	30	599
1700	31.5	584
2000	32.8	541

load is shown in Figure 4.4.

$$E = \frac{1}{2} C_L V_{in}^2 \tag{4.3}$$

$$P_{max} = \frac{dE}{dt} \tag{4.4}$$

$$P_{avr} = \frac{\Delta E}{\Delta t} \tag{4.5}$$

Since the output power had decreased dramatically from hundreds to a few μW, different rectifiers were employed to compare output power. Among these rectifiers, silicon diode rectifier MCC RB151 [40] provided highest value. Different capacitive and resistive load connections with MCC RB151 were tried to find out the maximum power that can be gained from polypropylene film harvester. The resistive load (optimal load, R_L = 1.273 MΩ) connected to the silicon diode rectifier MCC BR151 in parallel for the first configuration is shown in Figure 4.5.

The output power after rectification by the silicon diode rectifier MCC RB151, delivered

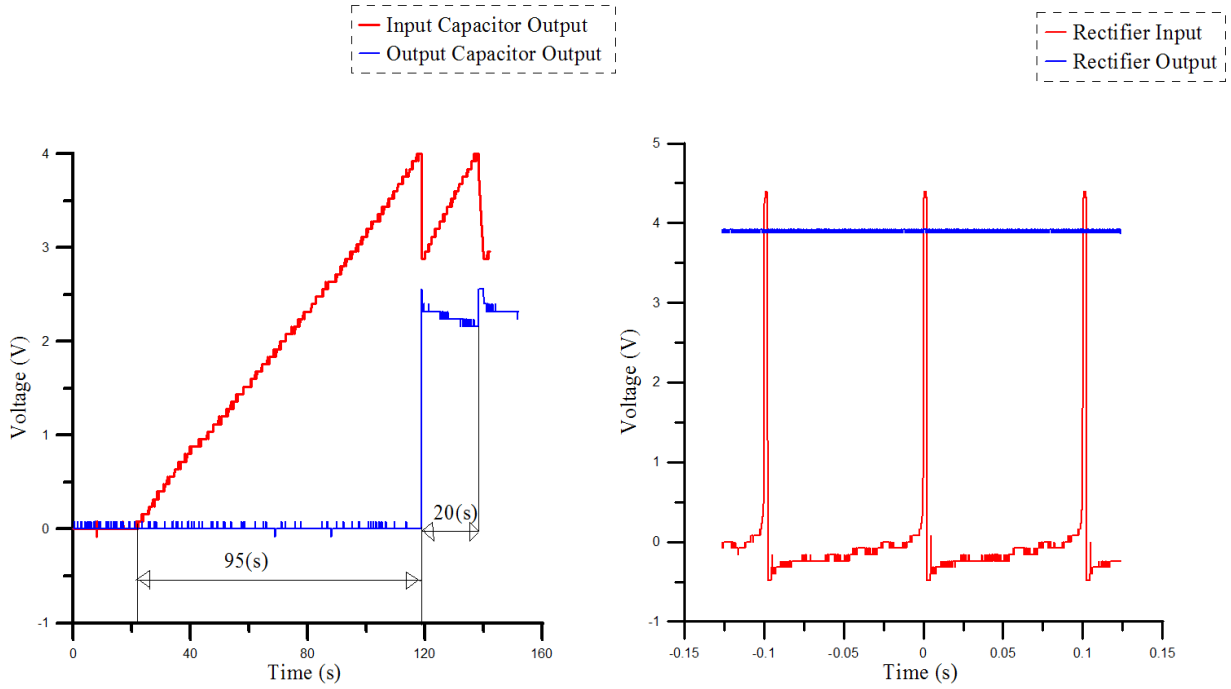

(a) With 94 μF. (b) Without load

Figure 4.4: PP harvester rectified output voltage of the by LTC3588-1 integrated circuit, red line is referred to V_{in}, blue line is referred to V_{out}.

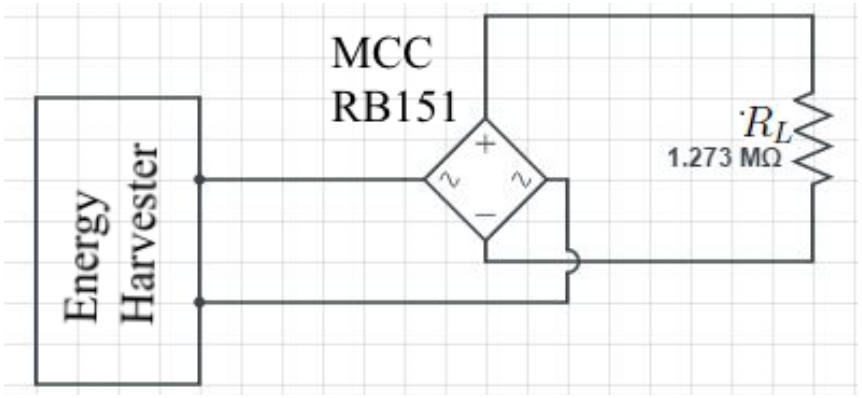

Figure 4.5: Schematic diagram of the resistive load connected to the silicon diode rectifier MCC RB151.

to R_L = 1.273 MΩ was 238 μW when the force was applied at 1 g acceleration while it was 513 μW (Equation 4.2 was used to calculate power) at 1.8 g acceleration as shown in Figure 4.7b. These power were calculated The output voltage is shown in Figure 4.6.

The instantaneous and average output power of the non-laminated PP on the resistor for both excitations was calculated. The results are shown in Figure 4.7.

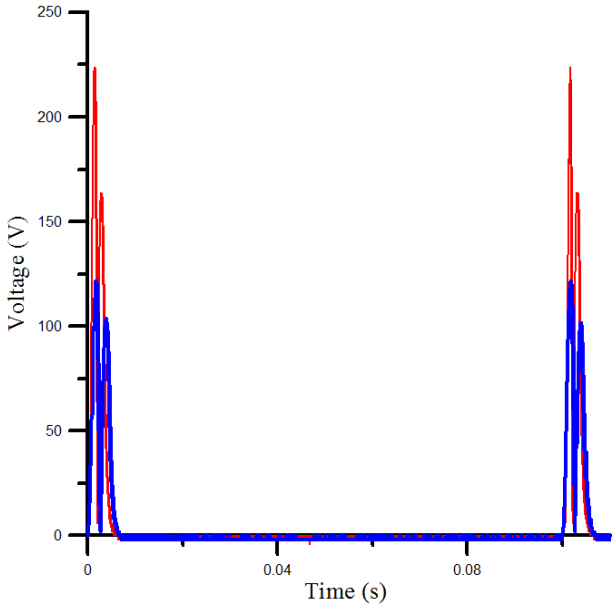

Figure 4.6: Non-laminated polypropylene harvester output voltage after rectification by the silicon diode rectifier MCC RB151, red line is referred to 1.8 g, blue line is referred to 1 g.

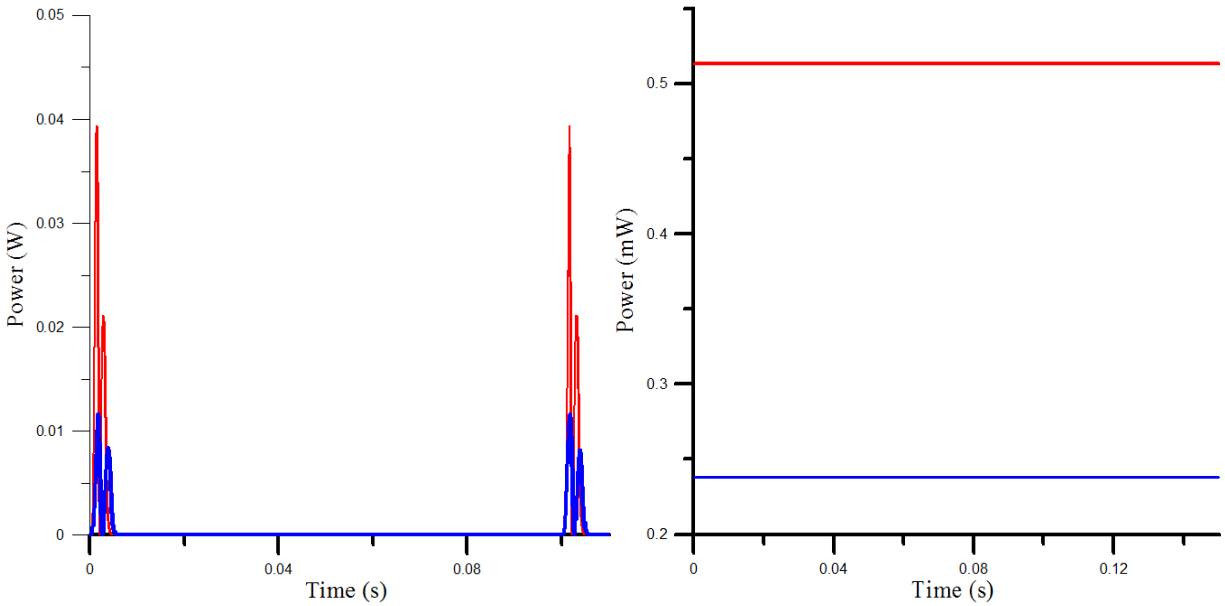

(a) Instantaneous power.

(b) Average power.

Figure 4.7: Non-laminated polypropylene harvester output power dissipated on the load R_L, 1.273 MΩ after rectification by MCC RB151, red line is referred to 1.8 g, blue line is referred to 1 g.

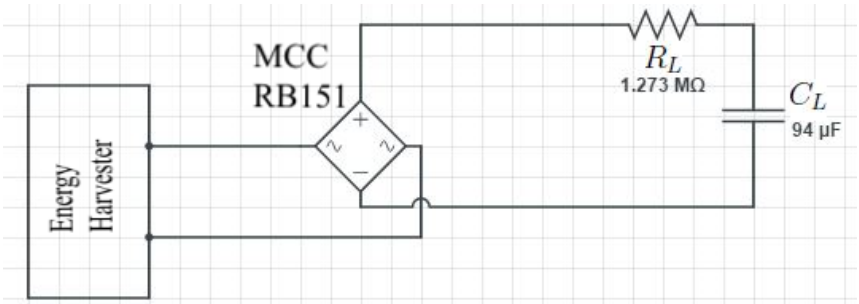

Figure 4.8: Schematic diagram of the capacitor and resistor after silicon diode rectifier MCC RB151.

The energy that was stored in the capacitor was calculated when the capacitor was connected in series with resistor after the silicon diode rectifier MCC RB151 for the second configuration is depicted in Figure 4.8.

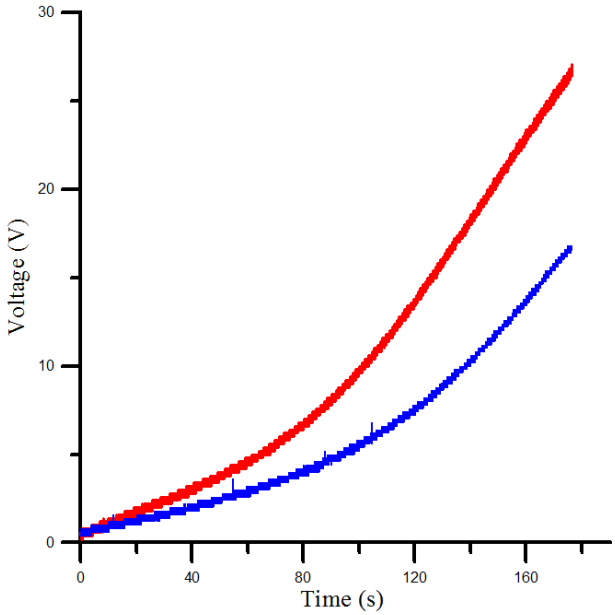

Figure 4.9: Non-laminated polypropylene harvester output voltage on the capacitor as function of time, red line is referred to 1.8 g, blue line is referred to 1 g accelerations.

The maximum output power (P_{max}) for the configuration of Figure 4.8 was calculated to be 143 μW when the resistor load was R_L = 1.273 MΩ and capacitive load is C_L=94 μF at 1 g acceleration and it was 380 μW at 1.8 g acceleration. The average power (P_{avr}) for both forces were 73.4 μW and 194 μW, respectively after three minutes testing. These power value were calculated in Equations 4.6 and 4.5. During test, the voltage reaches 16.6 V and 27 V for 1 g and 1.8 g respectively, as depicted in Figure 4.9. The open loop

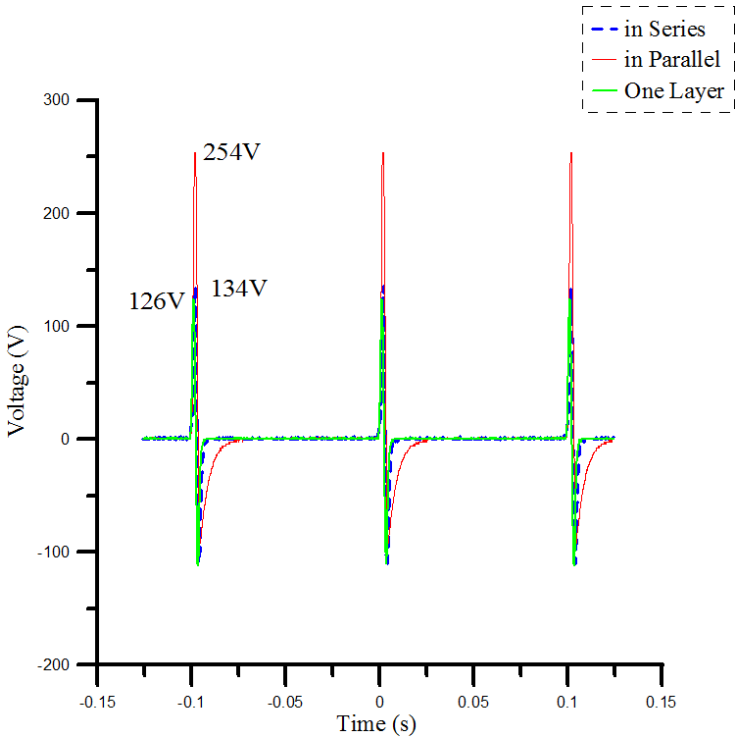

Figure 4.10: Non-laminated polypropylene harvester open loop output voltage as a function of time.

circuit voltage is shown in Figure 4.10. Experiment results show that the degradation is quite small for non-laminated PP. The open circuit voltage was 254 V at the beginning and it dropped to 240 V. PP harvester was tested during 3 months and 500 cycles per day.

4.2.1 Laminated PP

Laminated polypropylene harvester was tested at 1.8 g (m/s^2) acceleration. and 10 Hz. The output voltage was 19 V across the load (R_L) = 1.273 MΩ and output power was only 4 μW which is too low comparison to the non-laminated one. The rectified and non-rectified output voltage was shown in Figure 4.11a and the open loop circuit output voltage is shown in Figure 4.11b.

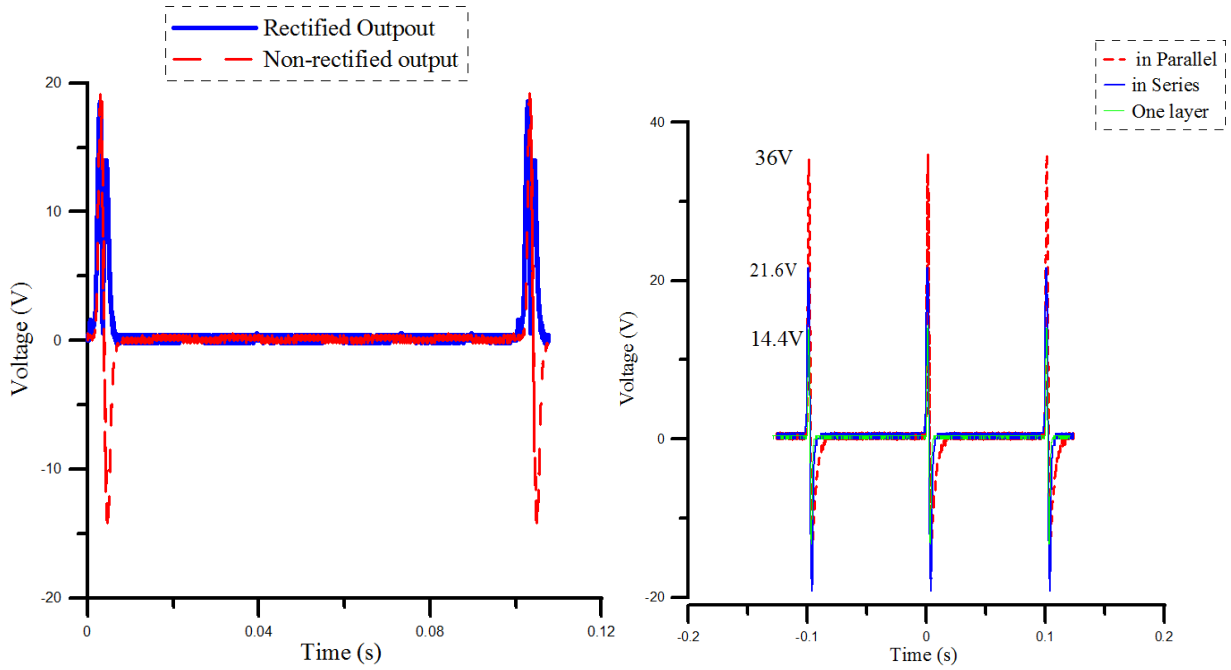

(a) Output voltage on the rsistor with and without rectifier, $R_L = 1.273$ MΩ.

(b) Open loop output voltage.

Figure 4.11: Laminated polyproplene harvester output voltage.

4.3 Piezoelectric Harvesters

The performance of the piezoelectric harvesters was tested by applying an acceleration of 1 g amplitude and frequencies of 10 Hz and 20 Hz. Harvesters were made out of eight layers of P(VDF-TrFE-CFE) connected in parallel. One harvester was tested in September, 2016. Its open circuit output voltage is shown in Figure 4.12 for an excitation frequency of 20 Hz. A second harvester was tested in April, 2017. Its open circuit output voltage is shown in Figure 4.13 for excitation frequencies 10 Hz and 20 Hz. It can observed from comparing these figures that the output voltage dropped from 8 V to less than 0.3 V over that period of time.

In comparison to the output voltage of ferroelectric harvesters, piezoelectric harvesters produced much less open circuit voltage and aged fast resulting in a further deterioration of their performance.

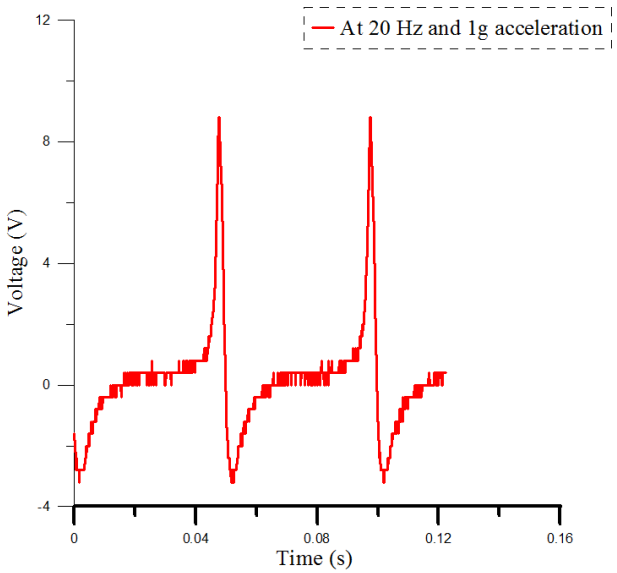

Figure 4.12: Output voltage of the PVDF harvester as a function of time.

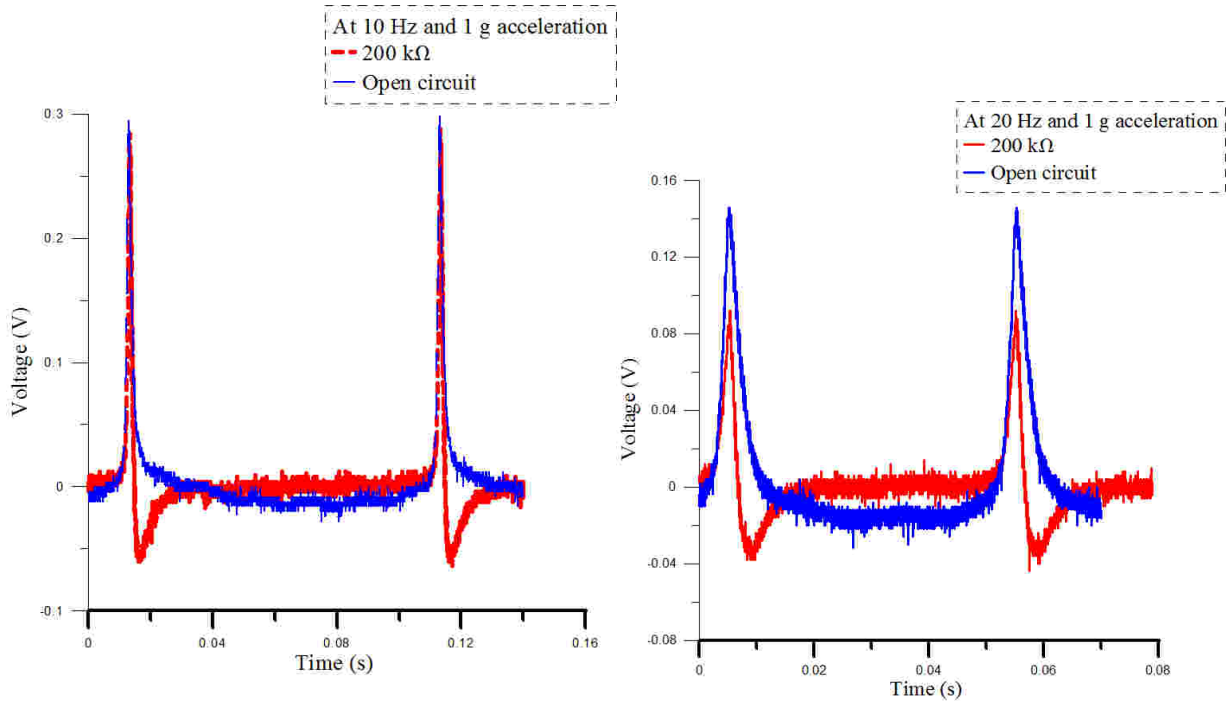

(a) (b)

Figure 4.13: Open circuit output voltage of the PVDF harvester as a function of time.

Table 4.2: The results of the PVDF harvester at 1 g acceleration.

	Acceleration (g)	Frequency (Hz)	Resistive load (kΩ)	Voltage (V)
September, 2016	1	20		8
April, 2017	1	10	200	0.288
April, 2017	1	20		0.3
April, 2017	1	20	200	0.142
April, 2017	1	20		0.09

4.4 Magnetostrictive Harvester

Figure 4.14 shows the output voltage of 0.17 mV after it was amplified by the gain of 90 with a 100 MΩ resistive load through instrument amplifier. This low output voltage is due to the fact that Terfenol-D is only suitable to be used at higher frequency [34, 35]. Also, Wang [34] have stated that for Terfenol-D to be used as energy harvester, a higher number of turns is required, which in this case is not possible due to the smaller size of Terfenol-D composite. At the same time, the linear coupling coefficient, d (Equation 1.6) for Terfenol-D composite is quite low, compared to its original materials (0.24 - 0.40 for Terfenol-D composite versus 0.70 - 0.80 for Terfenol-D) [17]. We concluded that Terfenol-D harvester would be more efficient in terms of output voltage when the density of Terfenol-D particles increased and excited at high frequency, which is not feasible for shoe.

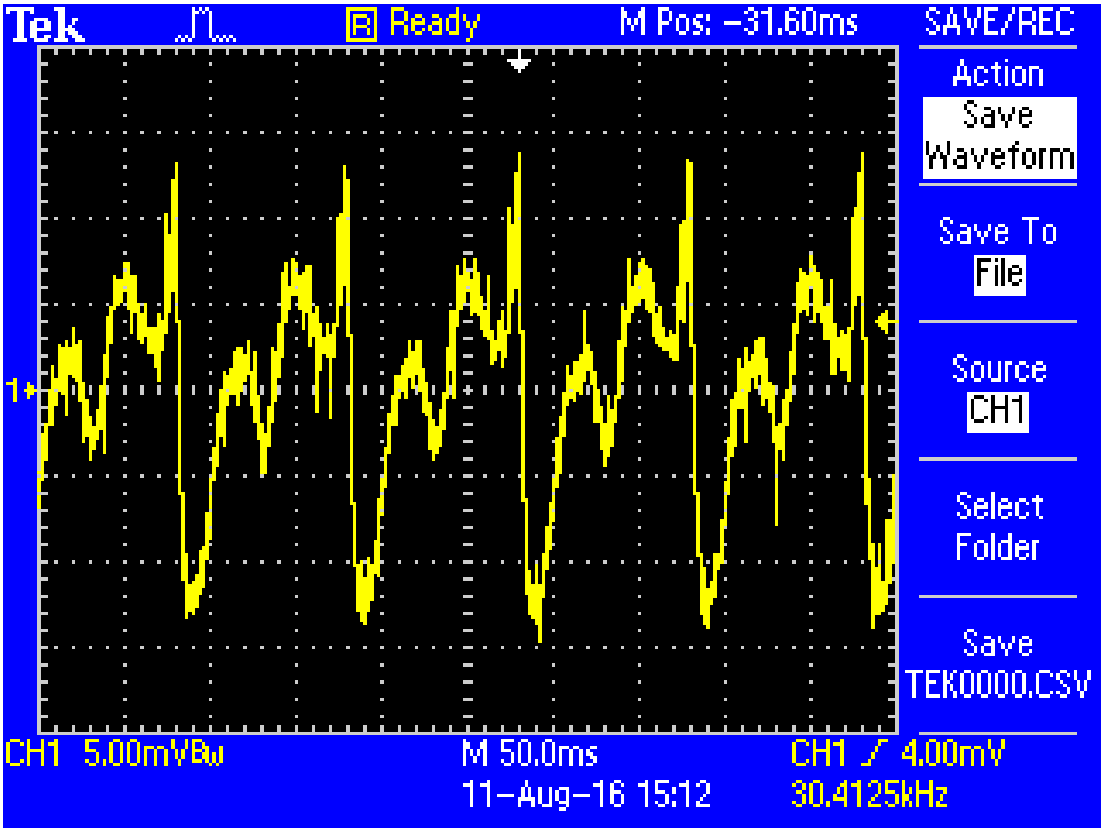

Figure 4.14: Terfenol-D harvester output voltage.

4.5 Summary

Three piezoelectric polymers and one magnetostrictive material were employed in this study. Two PP polymers were supplied without electrodes by EMFIT film. One of these polymers was laminated and another one was non-laminated. 3M copper conductive adhesive tape was employed as electrode and copper wire was soldered on the copper tape. Terpolymers of P(VDF-TrFE-CFE) was supplied by Piézotech S.A.S. with Cr/Au electrodes on both side. Although it had electrodes, but due to the material properties, we did not soldered copper wire onto the electrode because after certain temperature, the PVDF polymers start to degrade, which causes lose of the piezoelectric properties. Terfenol-D was supplied from ETREMA and two-component polyurethane (PU) resin (Smooth-Cast 60A) with low hardness was supplied by Smooth-On, Inc. To give flexibility and to avoid eddy current, Terfenol-D was compounded with PU.

The fact that we try to keep the harvester size small as much as possible is to preserve feasibility. The first prototype was designed in the size of 1 $\times$1 cm. However, since the output power was not desirable to power electronic devices, the size was changed to 1.6 $\times$1.6 cm. After deciding the dimension, several different methods were used to bond the insulator tape and double side tape. Firstly, the kapton tape was put on both sides of harvester unit as insulator, however when two sides insulated, the harvester unit became stiffer, which is undesirable. Because the strain that is created on the material will result in charge or voltage. The more strain, the more output. Then instead of insulating two sides, only one side is insulated with kapton tape and other harvester unit side was bonded with double side tape. Bonding each unit properly is important with regards to harvester efficiency. Since produced charges are proportional to the applied force on the energy harvester, proper bonding between layers will improve stress distribution on the energy harvester and it will also synchronize the charge transduction from the layers. If the layers are not attached to each other properly, the phase difference among them will decrease the efficiency.

For Terfenol-D harvester an aluminum mold was fabricated with three different sizes, $1\times1\times1$ cm, $1\times1\times0.5$ cm and $1\times0.5\times0.5$ cm to compare the ouput results according to

their sizes. As aforementioned, Terfenol-D and PU were combined and mixed for a while to obtain homogeneity. Then the mixture was casted and magnets were attached to both the mold sides. Magnets provide magnetic field to align the Terfenol -D particles and as a result, dipoles are created in the composite because after application of high magnetic field, particles are reoriented and even if the magnetic field is removed, particles will keep their alignment. Then the mold was placed in the oven for 24 hours to cure and displace the moisture from inside the composite. Then after curing process, copper wire is wounded around the harvester to capture the magnetic field change when the mechanical force is introduced.

The electromechanical model that we utilized was developed for PVDF and d_{31} mode, then it was converted to d_{33}, however, it did not work.

The optimal resistive load (R_L) was found as 1.273 MΩ and the RMS voltage V_{rms} was 28 V for the non-laminated PP harvester during testing at 2 g acceleration and 10 Hz. The output power delivered to the optimal load was 617 μW. The output power was decreased to 240 μW and 516 μW at 1 g and 1.8 g, respectively. Since the output power needed to be converted, the LTC3588-1 integrated circuit was used for that purpose. The maximum output power was 19 μW and 14.4 μW at 1 g and 1.8 g acceleration, respectively. Although it is expected that the energy stored in the capacitor is low, the output power of the LTC3588-1 was too low. The output power delivered to the load $R_L = 1.273$ MΩ was 238 μW when the force was applied at 1 g acceleration while it was 513 μW at 1.8 g acceleration when the silicon diode rectifier MCC RB151 was used instead of the LTC3588-1. After adding the capacitor to the MCC RB151, the maximum power P_{mx} was calculated as 143 μW and 380 μW for 1 g and 1.8 g accelerations, respectively. The average power P_{av} was calculated for both forces as 73.4 μW and 194 μW for 1 g and 1.8 g accelerations, respectively.

For the laminated PP harvester the results were quite low, where the voltage across to R_L was 19 V and the power delivered to the load R_L was 4 μW. The PVDF harvester output power was low as Terfenol-D harvester did so. The output results of harvesters were summarized in Table 4.3.

Table 4.3: The results of the harvesters at 1 g acceleration.

	N-laminated PP	Laminated PP	PVDF	Terfenol-D
$\text{Voltage}_{openLoop}$	254	36	8	0.17 mV
Power delivered to R_L	240 μW	4 μW	few nano W	

Chapter 5

Conclusions and Future Work

5.1 Discussion

The test results confirm that the output power is a function of input pressure force as noticed output power for the two force levels tested. The results show that the output power of the ferroelectric (PP) harvesters is one-order of magnitude higher than that of piezoelectric harvesters while the output power of magnetostrictive harvesters is marginal at less than 1 μW. The most important factor driving the difference in performance between ferroelectric and piezoelectric harvesters is the material piezoelectric constant (d_{33}). Piezoelectric constant of ferroelectrets (PP) is typically higher than that of PVDF. In our case, the piezoelectric constants of non-laminated and laminated PP are (d_{33}) = 300-400 pC/N, d_{33} = 25-30 pC/N. Another factor is Young's modulus in the strain direction. Young's modulus for non-laminated PP is more lower than that for laminated PP and PVDF [21, 28], thereby allowing for more strain (and more energy conversion) for a given pressure force.

The output power delivered to the storage capacitor was found to depend on the power management circuit used for rectification and regulation [9]. The efficiency of an off-the-shelf power management chip designed for energy harvesters, LTC3588-1, was found to be less than 10% while that of a custom circuit made of silicon diodes, bridge rectifier MCC RB151, and a switching power supply was found to be better than 90%. Since the available power is low, in the order of sub milliwatt, it is important to match the impedance

of the harvester to that of the power management circuit, to minimize ON-resistance, and current backflows. One reason behind the lower performance of the LTC3588 chip is the power consumption of on-board controller and other active components. Another reason is that the impedance profile of the LTC3588-1 chip is designed to match the impedance of piezoelectric harvesters. The PP harvester is ferroelectric with a much higher impedance. The impedance mismatch between the PP harvester and LTC3588-1 chip results in significant energy losses.

5.2 Conclusion and Recommendations

Wearable energy harvesting is in high demand as a power source for mobile electronic devices. Insole energy harvesting is one of the techniques to capture the human body motion and generate electrical energy. Our goal was to design and fabricate a practical shoe energy harvester. Four different prototypes were designed, fabricated, and tested employing PVDF, non-laminated PP, laminated PP, and Terfenol-D composite. We found that non-laminated PP shoe harvester is the most efficient in terms of power conversion efficiency and compatibility with shoe insole characteristics.

Power management plays a vital role in the overall efficiency of energy transduction. The efficiency of a custom-made power management circuit based on MCC RB151 silicon diodes bridge rectifier was found to be superior to that of the off-the-shelf LTC3588-1 power management chip. Further work is recommended to design and optimize power management circuits for ferroelectric harvesters.

The models tested in this project were found deficient. Effective models of shoe harvesters are another area of future research. Validated mathematical models, are necessary to reduce time and cost to develop energy harvesters into engineering practice. These models should enable engineers to select and tune the harvester design parameters.

References

[1] A. Erturk and D. J. Inman, "Piezoelectric energy harvesting", *John Wiley & Sons*, 2011.

[2] T. J. Kaźmierski, and S. Beeby, "Energy harvesting systems: principles, modeling and applications", *Springer Science & Business Media*,2010.

[3] R. Caliò, U. B. Rongala, D. Camboni, M. Milazzo, C. Stefanini, G. de Petris, and C. M. Oddo, "Piezoelectric energy harvesting solutions", *Sensor*, vol. 14, no. 3, pp. 4755–4790, 2014.

[4] Z. Yang, "High-performance Nonlinear Piezoelectric Energy Harvesting in Compressive Mode", *University of Toronto*, Phd Thesis, 2016.

[5] T. Starner, "Human-powered wearable computing", *IBM systems Journal* , vol. 35 no. 4, pp. 618–629, 1996.

[6] P. Niu, P. Chapman, R. Riemer, and X. Zhang, "Evaluation of motions and actuation methods for biomechanical energy harvesting", *Power Electronics Specialists Conference* ,PESC 04. 2004 IEEE 35th Annual, vol. 3, pp. 2100–2106, 2004.

[7] K. S. Ramadan, D. Sameoto, and S. Evoy, "A review of piezoelectric polymers as functional materials for electromechanical transducers", *Smart Materials and Structures*, vol. 23, no. 3, pp. 033001, 2014.

[8] R. Brown. "Power Generation Using Piezo Film", *Measurement Specialties, www.meas-spec.com* , no. 5, pp. 1-11.

[9] J. Granstrom, J. Feenstra, H. a Sodano, and K. Farinholt, "Energy harvesting from a backpack instrumented with piezoelectric shoulder straps," *Smart Mater. Struct.*, vol. 16, no. 5, pp. 1810–1820, 2007.

[10] J. J. Stroyan, "Processing and characterization of PVDF, PVDF-TrFE, and PVDF-TrFE-PZT composites", *Washington State University*, Master Thesis, 2004

[11] N. S. Shenck, "A demonstration of useful electric energy generation from piezoceramics in a shoe," *Massachusetts Institute of Technology, Dept. of Electrical Engineering and Computer Science*, Master Thesis, 1999

[12] J. S. Harrison and Z. Ounaies, "Piezoelectric Polymers", *Encyclopedia of Polymer Science and Technology*, 2002.

[13] F. Bauer, "Relaxor fluorinated polymers: novel applications and recent developments", *IEEE Transactions on Dielectrics and Electrical Insulation*, vol. 17, no. 4, 2010.

[14] C. Shafii, "Energy Harvesting using PVDF Piezoelectric Nanofabric", *University of Toronto*, Master Thesis, 2014.

[15] S. Bauer, R. Gerhard-Multhaupt, and G. M. Sessler, "Ferroelectrets: Soft electroactive foams for transducers", *Physics Today*, vol. 57, no. 2, pp. 37–43, 2004.

[16] F. T. Calkins, A. B. Flatau, and M. J. Dapino, "Overview of magnetostrictive sensor technology," *Journal of Intelligent Material Systems and Structures*, vol. 18, no. 10, pp. 1057–1066, 2007.

[17] I. D. Mayergoyz G. Engdahl, "Handbook of giant magnetostrictive materials," *Elsevier*, 1999.

[18] C. Rodriguez, M. Rodriguez, I. Orue, J. L. Vilas, J. M. Barandiarán, M. L. F. Gubieda, L. M. Leon, "New elastomer–Terfenol-D magnetostrictive composites," *Sensors and Actuators A: Physical*, vol. 149, no. 2, pp. 251–254, 2009

[19] J. Zhai, "Magnetoelectric laminated composites and devices", *Virginia Polytechnic Institute and State University*, Phd Thesis, 2009.

[20] C. RodrÃguez, A. Barrio, I. Orue, J. L. Vilas, L. M. León, J. M. Barandiarán, and M.L. Fdez-Gubieda Ruiz, "High magnetostriction polymer-bonded Terfenol-D composites," *Sensors and Actuators A: Physical*, vol. 142, no. 2, pp. 538–541, 2008.

[21] N. S. Shenck and J. A. Paradiso, "Energy scavenging with shoe-mounted piezoelectric," *IEEE micro*, vol. 21, no. 3, pp. 30–42, 2001.

[22] Y. Xin, X. Li, H. Tian, C. Guo, C. Qian, S. Wang, C. Wang, "Shoes-equipped piezoelectric transducer for energy harvesting: A brief review," *Ferroelectrics* , vol. 493, no. 1, pp. 12–24, 2016.

[23] J. G. Rocha, L. M. GonÃ§alves, P. F. Rocha, M. P. Silva, and S. Lanceros-Méndez, "Energy harvesting from piezoelectric materials fully integrated in footwear," *IEEE transactions on industrial electronics*, vol. 57, no. 3, pp. 813–819, 2010

[24] J. Zhao and Z. You, "A shoe-embedded piezoelectric energy harvester for wearable sensors," *Sensors (Basel), Switzerland*, vol. 14, no. 7, pp. 12497-12510, 2014.

[25] T. Kanchan, K. Krishan, D. Prusty, and M. Machado, "Heel–Ball index: An analysis of footprint dimensions for determination of sex", *Egyptian Journal of Forensic Sciences*, vol. 4, no. 2, pp. 29–33, 2014.

[26] J. Zhao and Z. You, "Models for 31-mode PVDF energy harvester for wearable applications," *Sci. World J*, vol. 2014, 2014.

[27] Z. Luo, D. Zhu, and S. Beeby, "An electromechanical model of ferroelectret for energy harvesting," *Smart Materials and Structures* , vol. 25, no. 4, pp. 045010, 2016.

[28] S. Anton, K. Farinholt, and A. Erturk, "Piezoelectret foam–based vibration energy harvesting," *Journal of Intelligent Material Systems and Structures*, vol. 25, no. 14, pp. 1681–1692, 2014.

[29] D. Fourie, "Shoe mounted PVDF piezoelectric transducer for energy harvesting," 2010.

[30] Z. Luo, D. Zhu, J. Shi, S. Beeby, C. Zhang, P. Proynov, and B. Stark, "Energy harvesting study on single and multilayer ferroelectret foams under compressive force," *IEEE Transactions on Dielectrics and Electrical Insulation*, vol. 22, no. 3, pp. 1360–1368, 2015.

[31] Z. Luo, D. Zhu, and S. P. Beeby, "Multilayer ferroelectret-based energy harvesting insole," *Journal of Physics: Conference Series*, vol. 660, no. 1, pp. 012118, 2015.

[32] C. A. Ray, S. R. Anton, "Multilayer piezoelectret foam stack for vibration energy harvesting," *Journal of Intelligent Material Systems and Structures*, pp. 1045389X16657420, 2016

[33] M. E. Staley, A. B. Flatau, "Characterization of energy harvesting potential of Terfenol-D and Galfenol," *Smart Structures and Materials*, pp. 630–640, 2005

[34] L. Wang and F. G. Yuan, "Vibration energy harvesting by magnetostrictive material," *Smart Materials and Structures*, vol. 17, no. 4, pp. 045009, 2008.

[35] V. Berbyuk and J. Sodhani, "Towards modelling and design of magnetostrictive electric generators," *Computers & structures*, vol. 86, no. 3, pp. 307–313, 2008.

[36] L. A. Dobrzański, A. E. Tomiczek, A. W. Pacyna, "Properties of the magnetostrictive composite materials with the polyurethane matrix reinforced with Terfenol-D particles," *Manufacturing Engineering*, vol. 55, no. 2, pp. 316–322, 2012.

[37] B. Tunkar, "Electromagnetic Vibrational Energy Harvesters and Power Management," *University of Waterloo*, Master Thesis, 2016.

[38] http://www.linear.com/product/LTC3588-1.

[39] https://www.interlinkelectronics.com/datasheets/ DatasheetFSR .pdf

[40] http://www.mouser.com/ds/2/258/RB151-RB157(RB-15)-480662.pdf